TÉCNICO
LISBOA

Stimuli responsive surfactants: towards smart templates for mesoporous silica nanoparticles

Inês Rodrigues Marta dos Santos

Thesis to obtain the Master of Science Degree in

Chemistry

Supervisors: Prof. Dr. Carlos Miguel Calisto Baleizão

Prof. Dr. José Paulo Sequeira Farinha

Examination Committee

Chairperson: Prof. Dr. Isabel Maria Delgado Jana Marrucho Ferreira

Supervisor: Prof. Dr. Carlos Miguel Calisto Baleizão

Members of the Committee: Prof. Dr. João Paulo Costa Tomé

November 2022

Declaration

I declare that this document is an original work of my own authorship and it fulfills all the requirements of the Code of Conduct and Good Practices of the Universidade de Lisboa.

Acknowledgments

As this master's thesis is coming to an end, I want to thank everyone who contributed to this thesis and helped make this journey a more enjoyable and enriching process. I must start by thanking my supervisors, Prof. Dr. José Paulo Sequeira Farinha and Prof. Dr. Carlos Miguel Calisto Baleizão, for the opportunity to work on this project and for all the guidance, help, and knowledge they shared with me during these months.

I would also like to thank all my lab colleagues for always being available to help and for having the patience to answer all my questions. To Dr. Ermelinda Maçoas, for taking her time to explain and help me with the computational studies. To Prof. João Tomé, for opening the doors of his laboratory, for all his availability and kindness in welcoming me.

Finally, I must give a huge thank you to my boyfriend, friends, and family for their constant love, support, and strength they gave me during this time.

Abstract

Mesoporous silica nanoparticles (MSNs) feature unique characteristics that make them useful in multiple applications. Novel MSNs with a dual pore system, containing two distinct types of pores that can carry and independently deliver different cargo at the same time, would open even greater possibilities from catalysis to sensing, energy, biomedicine, etc.

To develop dual pore system MSNs an innovative strategy is presented in this work based on a system of two surfactants that do not interfere with each other forming mixed micelles and that could be removed selectively allowing pore functionalization and selective control release. Our approach is to develop novel cleavable surfactants that can be selectively removed through a specific stimulus. Two possible structures for the cleavable surfactant are proposed in this work: a light responsive surfactant and a redox responsive surfactant.

The redox responsive surfactant (CTAC-SS) was successfully obtained in moderate to high yields, and some preliminary studies were conducted to evaluate its behavior as a smart surfactant. Degradability tests were conducted, and after 30 minutes in the presence of dithiothreitol (DTT), it was possible to observe the characteristic absorption band of *ox*-DTT at 283 nm, which is an indicator of the effective response of CTAC-SS to the stimulus. An estimate critical packing parameter of CTAC-SS was obtained from its optimized structure, and the result indicate that CTAC-SS will form cylindrical micelles, due to the structure similarity with CTAB. Surface tension of a set of solutions of CTAC-SS was measured using the pendant drop method, however the results were not conclusive on the behavior of CTAC-SS in solution and was not possible to determine the critical micelle concentration (CMC). DLS results of CTAC-SS solutions reveal the presence of particles with 47 ± 5 nm of mean hydrodynamic diameter, which, if cylindrical micelles are formed as predicted by the cpp, correspond to the formation of cylindrical micelles with a maximum length of 261 nm.

Overall, the results indicate that our goal was met with the production of CTAC-SS, which can be a promising smart surfactant with broad applications, including the synthesis of dual pore MSNs and other nanostructures.

Keywords: mesoporous silica nanoparticles, dual pore system, stimuli responsive surfactant, selective template removal, selective functionalization

Resumo

As nanopartículas de sílica mesoporosa (MSNs) apresentam características únicas que as tornam úteis em múltiplas aplicações. Novas MSNs com um sistema de duplo poro, contendo dois tipos distintos de poros que podem transportar e entregar cargas diferentes de forma independente ao mesmo tempo, abririam novas possibilidades em áreas como catálise, energia, biomedicina, etc.

Para desenvolver as MSNs com sistema de duplo poro, apresenta-se uma estratégia inovadora neste trabalho baseada num sistema de dois surfactantes que não interferem entre si, formando micelas mistas, e que podem ser removidos seletivamente permitindo a funcionalização dos poros e libertação seletiva. A nossa abordagem é desenvolver novos surfactantes cliváveis que podem ser removidos seletivamente através de um estímulo específico. Duas estruturas possíveis para o surfactante clivável são propostas neste trabalho: um surfactante responsivo à luz e um surfactante redox responsivo.

O surfactante redox responsivo (CTAC-SS) foi obtido com sucesso, com rendimentos moderados a altos, e alguns estudos preliminares foram realizados para avaliar o seu comportamento como surfactante inteligente. Uma estimativa do parâmetro crítico de empacotamento do CTAC-SS foi obtida a partir da sua estrutura otimizada, e os resultados indicam que o CTAC-SS formará micelas cilíndricas, devido à similaridade de estrutura com o CTAB. Foram realizados testes de degradação, e após 30 minutos na presença do ditiotreitol (DTT), foi possível observar a banda de absorção característica do *ox*-DTT a 283 nm, que é um indicador da resposta efetiva do CTAC-SS ao estímulo. A tensão superficial de um conjunto de soluções de CTAC-SS foi medida pelo método da gota pendente, porém os resultados não foram conclusivos sobre o comportamento do CTAC-SS em solução e não foi possível determinar a concentração micelar crítica (CMC). Os resultados de DLS das soluções de CTAC-SS revelam a presença de partículas com 47 ± 5 nm de diâmetro hidrodinâmico médio, que, se as micelas cilíndricas forem formadas como previsto pelo cpp, correspondem à formação de micelas cilíndricas com um comprimento máximo de 261 nm.

No geral, os resultados indicam que nosso objetivo foi alcançado com a produção de CTAC-SS, que pode ser um surfactante inteligente promissor com vastas aplicações, incluindo na síntese de MSNs de duplo poro e para outras nanoestruturas.

Palavras-chave: partículas de sílica mesoporosa, sistema de duplo poro, surfactantes responsivos, remoção seletiva, funcionalização seletiva

Contents

Figures Index

easily inside the pores) and **(B)** a redox responsive group (cleaved by DTT, a small molecule) as linkers. Both structures guarantee the stability of the surfactant during the MSNs synthesis and the selective removal of the cleavable surfactant through a specific stimulus. These surfactants should form cylindrical micelles and avoid the formation of mixed micelles with the second surfactant. 19

Tables Index

Abbreviations List

2-DAT	2-(dimethylamino) ethanethiol
ATR-FTIR	Attenuated total reflectance - Fourier transform infrared spectroscopy
BAC	Benzalkonium chloride
CMC	Critical Micelle Concentration
CPC	Cetylpyridinium chloride
cpp	Critical Packing Parameter
CTAB	Cetyltrimethylammonium bromide
DDAC	Didecyldimethylammonium chloride
DLS	Dynamic Light Scattering
DpSN	Dual-sized pore silica nanoparticle
DTT	Dithiothreitol
DTT	Dithiothreitol
FDA	Food and Drug Administration
GRAS	Generally Recognized as Safe
HFDePC	1H1H2H2H-perfluorodecylpyridinium chloride
HSQC	Heteronuclear single quantum coherence spectroscopy
Hz	Hertz
IL	Ionic Liquid
LSB	Lauryl sulfate betaine
m/z	Mass to charge ratio
MCM	Mobil Crystalline Material or Mobil Composition of Matter
MSN	Mesoporous Silica Nanoparticle
NMR	Nuclear Magnetic Resonance Spectroscopy
ONV	α-methyl-*o*-nitroveratryl
PS-b-PAA	Polystyrene-b-poly (acrylic acid)
R_g	Radius of gyration
R_H	Hydrodynamic radius
SBA	Santa Barbara Amorphous
SDA	Structure Directing Agent
SDS	Sodium dodecyl sulfate
SNP	Silica Nanoparticle
SpSN	Single pore silica nanoparticle
TAB	(3-bromopropyl) trimethylammonium
TBOS	Tetrabutyl orthosilicate
TEA	Triethylamine

TEOS   Tetraethyl orthosilicate

THEOS   Tetrakis(2-hydroxyethyl) orthosilicate

TMOS   Tetramethyl orthosilicate

TMVS   Tetramethoxy vinylsilane

1. Introduction

Silica is one of the most abundant minerals in the Earth's crust appearing in different areas of our daily life throughout history integrating materials such as glass, concrete, vitroceramics, plastics, paper, paints, semiconductors, and others. Amorphous silica and silicates are generally recognized as safe (GRAS) by the US Food and Drug Administration (FDA).[1]

The emergence of nanotechnology allowed the manipulation of matter at the nanoscale (1–100 nm) taking advantage of the unique properties of nanomaterials (materials that have at least one dimension in the nanoscale), leading to a transformation in science, engineering, and technology.[2,3] Silica nanoparticles (SNPs) were part of this evolution and are now widely used in agriculture, food industry, biomedical applications, and industrial applications.[1,4]

Silica nanoparticles stand out because of their unique and controllable characteristics such as tunable size, porosity, and shape.[5] Their optical properties, high surface area, hydrophilicity, biocompatibility, and low toxicity, conjugated with the possibility of functionalization and encapsulation of compounds, makes them especially useful in biomedicine, as carriers for drug and gene delivery, for sensing and imaging diagnosis.[4,5]

1.1. Synthesis of Silica Nanoparticles

Silica nanoparticles (SNPs) used in scientific applications cannot be extracted from natural sources, so they must be synthesized. Two different approaches can be used to synthesize SNPs: top-down and bottom-up approaches. In top-down approach the dimension of the original material must be decreased in size by special size reduction techniques. Bottom-up or chemical approach starts from individual atoms or molecules to produce particles of a desired size.[2,3,6,7] This method allows greater precision, size regularity, and homogeneity of the final product, although it involves higher costs.[6] Some of the widely used methods to synthesize silica nanoparticles are reverse microemulsion, flame synthesis (or chemical vapor condensation), and sol-gel process, which is the most common method.[3]

1.1.1 Sol-gel and Stöber Methods

The sol-gel method can be used to build materials with controlled structures and properties, such as bulk gels, films, powders, and nanoparticles, that are employed in several areas, like energy, aerospace, optics, sensors, electronics, medicine, and others (**Figure 1**).[8,9]
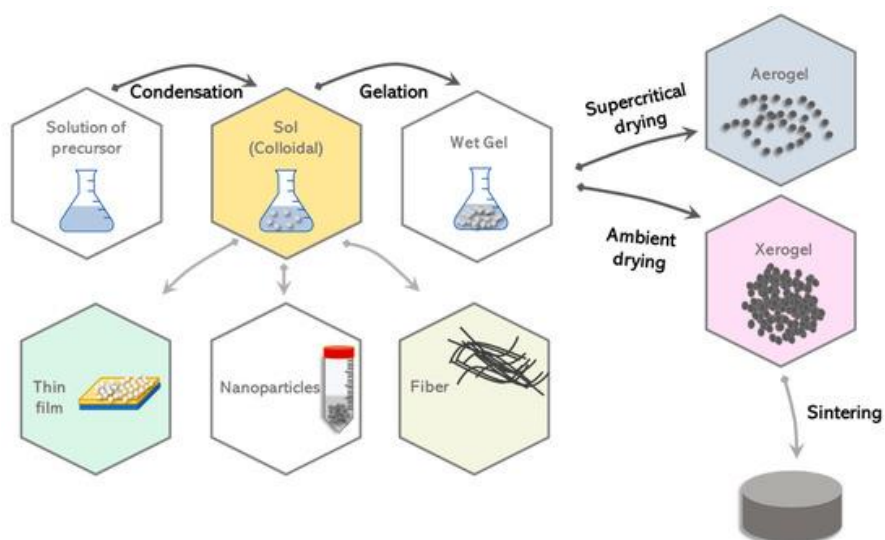
Figure 1. *Representation of different materials obtained using the sol-gel method. Adapted from 8.*

The sol-gel procedure is the most used method to synthesize silica nanoparticles due to its low cost, low temperature conditions and simple procedure, allowing the production of high quality silica nanoparticles at an industrial scale.[10,11] In this process, a silicon ester used as silica precursor ($Si(OR)_4$) reacts with water (hydrolysis) to form silanol groups (Equation 1) which then condensate leading to the creation of siloxane (Si-O-Si) bonds (Equation 2 and 3) that interact cooperatively to produce a colloidal suspension of particles in a liquid (sol), followed by the formation of a continuous network (gel) (**Figure 1**).[1,3,8,9,12,13] This method uses a catalyst (a base or an acid) that can affect the hydrolysis and condensation rates and the structure of the final product.[8] The acid catalysis results in weakly cross-linked linear polymers, due to the low condensation kinetic rate at low pH and poor solubility of silica oxide in acid medium. While in basic conditions the kinetic rates of hydrolysis and condensation are faster allowing the formation of highly branched clusters.[12–14]

$$\underset{\underset{OR}{|}}{\overset{\overset{OR}{|}}{RO-Si-OR}} + H_2O \xrightarrow{\text{Hydrolysis}} \underset{\underset{OR}{|}}{\overset{\overset{OR}{|}}{HO-Si-OR}} + ROH \qquad (1)$$

$$\underset{\underset{OR}{|}}{\overset{\overset{OR}{|}}{RO-Si-OR}} + \underset{\underset{OR}{|}}{\overset{\overset{OR}{|}}{HO-Si-OR}} \xrightarrow{\substack{\text{Alcohol} \\ \text{Condensation}}} \underset{\underset{OR}{|}\;\;\underset{OR}{|}}{\overset{\overset{OR}{|}\;\;\overset{OR}{|}}{RO-Si-O-Si-OR}} + ROH \qquad (2)$$

$$\underset{\underset{OR}{|}}{\overset{\overset{OR}{|}}{RO-Si-OH}} + \underset{\underset{OR}{|}}{\overset{\overset{OR}{|}}{HO-Si-OR}} \xrightarrow{\substack{\text{Water} \\ \text{Condensation}}} \underset{\underset{OR}{|}\;\;\underset{OR}{|}}{\overset{\overset{OR}{|}\;\;\overset{OR}{|}}{RO-Si-O-Si-OR}} + H_2O \qquad (3)$$

2
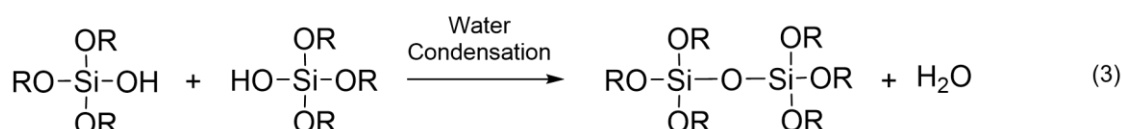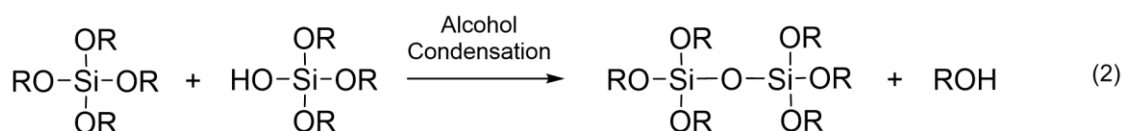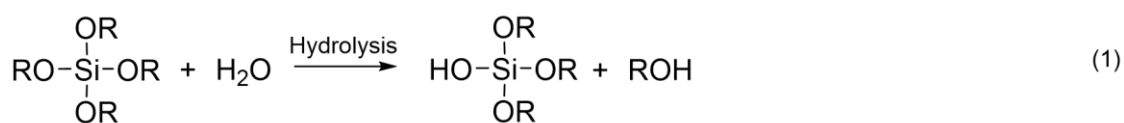
The controlled aggregation model has been proposed to describe the growth mechanism of silica. It states that the formation of silica particles can be separated into two steps: nucleation and growth. Nucleation takes place after the condensation of monomers into a polymeric structure. The nuclei created are colloidally unstable and susceptible to aggregation, leading to the formation of primary particles. These primary particles aggregate to form larger particles, designated secondary particles, until a certain size (colloidally stable) is reached.[3,15]

Stöber was the first to develop a method based on a sol-gel process to synthesize (quasi)monodisperse colloidal suspensions of nonporous silica spheres in the range of 0.05 to 2 μm. The method involves the hydrolysis and condensation of tetraallyl orthosilicates under mild conditions (room temperature, pH 9-11) in the presence of a mixture of alcohol and water, using ammonia as catalyst to accelerate the rate of hydrolysis and condensation. The OH$^-$ ions present in the ammonia solution are stronger nucleophiles than water, attacking ethoxy groups (Si-OR) more easily.[1,12,15–17] Since 1968, when Stöber revealed the synthetic procedure, several modifications have been made to synthesize monodisperse and ordered silica particles with different shapes and sizes ranging from tens of nanometers to few microns.[12,16,17] By changing the reaction conditions such as the type of tetraalkyl orthosilicate, the concentration of ammonia and the alcoholic solvent, it is possible to obtain particles with different sizes, as indicated in **Figure 2**.[12]

Reduction of particle size

Alkyl silicates (Si(OR)$_4$, R=Me, Et, Pr and Bu)

TBOS (R=Bu)   TMOS (R=Me)

Ammonia concentration (pH)

High   Low

Alcoholic solvents

n-BuOH   MeOH
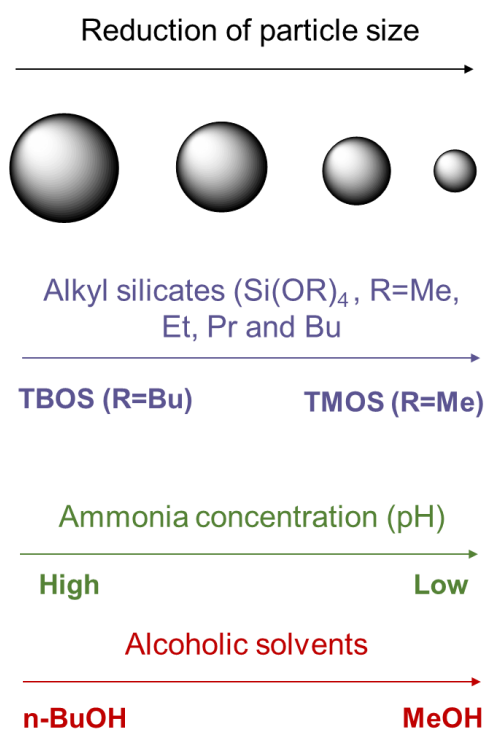
Figure 2. Schematic representation of the effect of different reaction parameters on the size of spherical silica nanoparticles prepared by the Stöber method. Adapted from 16.

The pH affects profoundly the reaction kinetics since both hydrolysis and condensation depend on the charge of silica species. Below the isoelectric point of silica (IEP=2.0), the silica species are positively charged ($SiOH_2^+$), and the charge density increases as the pH decreases. At this point the hydrolysis rate reaches a maximum value and decreases until it reaches a minimum value at neutral pH (red curve in **Figure 3**). Above the IEP the silica species are negatively charged (SiO^-) and the hydrolysis rate increases along with the pH. The condensation rate (green curve in **Figure 3**) has its minimum at the IEP of silica and has a maximum value at pH=7.5, decreasing for pH>7.5, because the silicates start to dissolve. This implies that at higher values of pH both hydrolysis and condensation kinetic rates are higher and the particles obtained have larger sizes, in fact the pH (catalyst concentration) is the dominant factor influencing the particle size (**Figure 3**).[12,17–21]
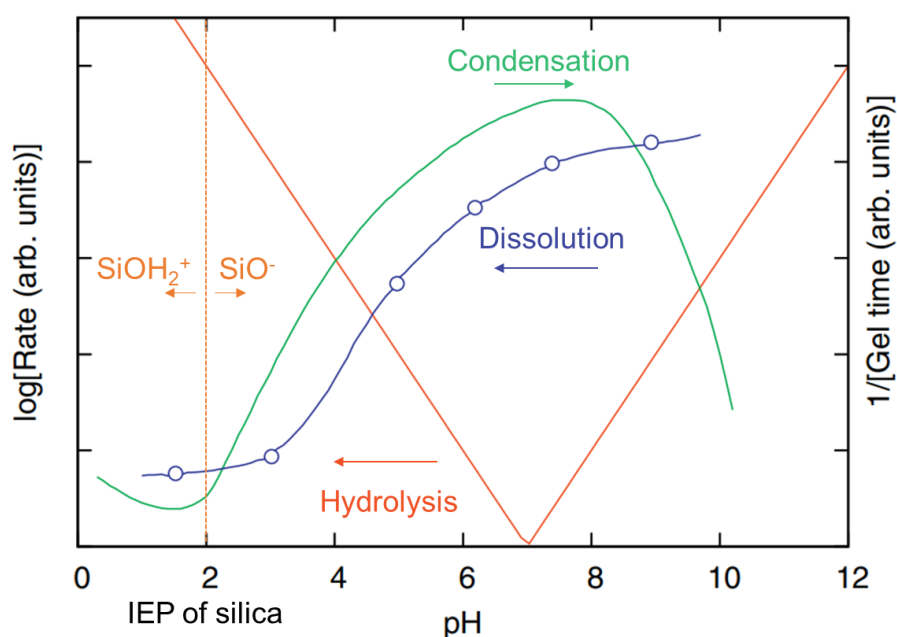
Figure 3. *Effects of the pH on the silica hydrolysis (red), condensation (green) and dissolution (blue) rates. Adapted from 19.*

Other factors can be determinant to define the size of the particle, for example, tetraalkyl orthosilicates originate particles of different sizes. The particle size increases for precursors with larger and/or branched chains, due to steric effects that lower the hydrolysis rate, as represented in **Figure 2**, comparing TMOS (smaller alkyl chain size, with only one carbon) with TBOS (alkyl chain containing four carbon atoms).[12,17] Chiang et al.[18] also found that the particle size increases as the concentration of TEOS (silica precursor) increases. Higher temperatures increase the hydrolysis rate resulting in the creation of more nucleation points, leading to the formation of smaller particles.[17,18] The rates of hydrolysis and condensation of TEOS strongly depends on the solvent properties like polarity, steric hindrance and viscosity, thus the size of the particles also varies by changing solvent properties.

Although an exact relation between particle size and solvent properties is not well establish, typically it is noted that by decreasing the alkyl chain size of the alcohol, polarity increases and viscosity decreases, leading to a decrease in the particle size, as shown in **Figure 2**.[22]

1.2. Mesoporous Silica Nanoparticles

Mesoporous Silica Nanoparticles (MSNs) are porous solid materials with inorganic siloxane structures and tunable pore diameters in the range of 2–50 nm.[23,24] MSNs are considered interesting materials in the nanotechnology field due to their unique characteristics that make them useful to employ in multiple fields.[17,24] MSNs are non-toxic, chemically inert, biocompatible, thermal and mechanically stable. MSNs possess high internal surface area and controllable pore volume, colloidal stability, and the possibility of selectively functionalize the internal (pore) and external surfaces.[13,17,24,25] Their accessible and unique pore structure can host and release a large variety of molecules and therapeutic agents at specific locations.[13,17] MSNs are easy to synthesize and inexpensive, which along with other suitable characteristics, makes them attractive materials in areas like catalysis (acting as solid supports to accommodate active sites), biomedicine, sensing, energy, etc.[17,24]

1.2.1. Syntheses of Mesoporous Silica Nanoparticles

Although the synthesis of mesoporous silica nanoparticles dates from the 1970s, only in 1988 the idea of surfactant templating to produce mesoporous silica nanoparticles was reported by Kuzuyuki Kuroda et al.[26] Followed by Mobil Research and Development Corporation researchers that synthesised for the first time mesoporous silica solids from aluminosilicate gels using a crystal template mechanism, in 1992. This new family of mesoporous silica nanoparticles was designated as MCMs (Mobil Crystalline Materials or Mobil Composition of Matter).[12,13,24] The most common are MCM-41 particles which have an hexagonal arrangement and pores of 2.5 to 6 nm, MCM-48 has a cubic arrangement and MCM-50 has a lamella-like arrangement.[17] Another type of MSNs was developed by University of California, Santa Barbara, and named Santa Barbara Amorphous type material (SBA). This type of particles uses non-ionic triblock copolymers like alkyl poly(ethylene oxide) oligomeric surfactants and poly(alkylene oxide) block copolymers as templates. Based on the symmetry of the mesoporous structure and the type of template used, different types of SBA particles can be obtained: SBA-11 (3D cubic), SBA-12 (3D hexagonal), SBA-15 (2D hexagonal) and SBA-16 (cubic). SBA particles differ from MCMs due to their larger pores of 5 to 30 nm and thicker silica walls.[12,13,24] In **Figure 4** are represented different types of MSNs, including FDU-2 and KIT-5 types.[12,27]
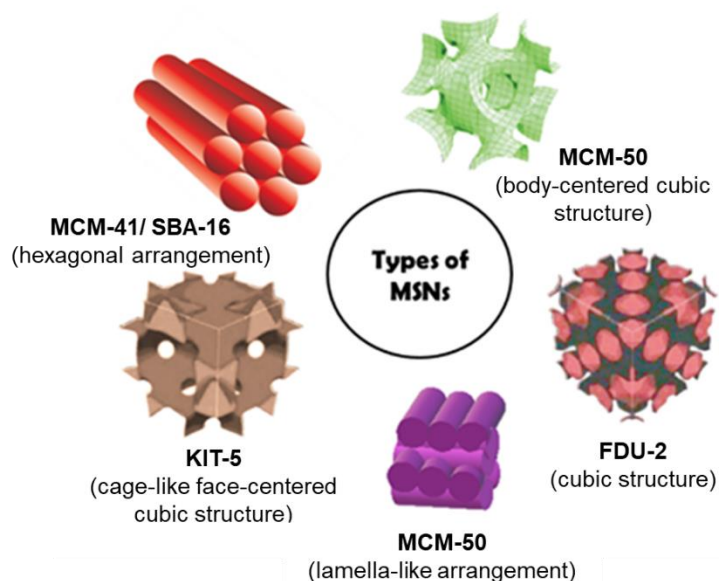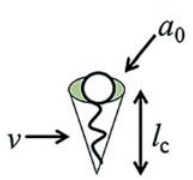
Figure 4. Representation of different types of MSNs.(Adapted from 12)

Grun et al. was the first to modify the Stöber method by using a cationic surfactant as template to produce submicrometric-scaled MCM-41 spherical particles. Since then, several modifications to the Stöber synthetic procedure have been made. Different reaction mixtures and different templates have been used to formulate MSNs with different pore sizes and different mesostructures. Later the term MSN was popularized by Victor Lin to represent mesoporous silica nanospheres.[17] Currently, almost all MSNs are prepared using various modifications of the Stöber method.[13,17,25] The synthesis of ordered mesoporous spherical silica nanoparticles using the Stöber modified method rely on the addition of a new reactant to the system, that already contains a silica precursor (tetraethyl orthosilicate-TEOS, tetramethyl orthosilicate-TMOS, tetramethoxyvinylsilane- TMVS, sodium meta-silicate or tetrakis(2-hydroxyethyl) orthosilicate- THEOS) and a catalyst. This new reactant is a surfactant (template) that acts as a structure directing agent (SDA), consisting of a hydrophilic and a hydrophobic group.[12,16]

In the case of MCM-41 type materials, the surfactant used is generally a tetraalkyl ammonium cation with a hydrophobic alkyl chain (for example, CTAB) that forms cylindrical micelles with an inner core containing the hydrophobic parts, at concentrations higher than the critical micelle concentration (CMC), through a process regulated by hydrophobic interactions.[20,24] To obtain cylindrical micelles the surfactant must have a critical packing parameter (cpp) between 0.33 and 0.5, which is determined using Equation 4, where v is the volume of the hydrophobic part, a_0 is the area of the hydrophobic/hydrophilic interface and l_c is the length of the hydrophobic part. By changing the values for the parameters described in Equation 4, it is possible to obtain different types of micelle structures such as spherical micelles, cylindrical micelles, bilayers, inverted micelles, etc, as shown in **Figure 5**.[28]

$$cpp = \frac{v}{a_0 l_c} \qquad (4)$$

Figure 5. *Different micelle structures obtain by variation of the critical packing parameter (cpp). Adapted from 28.*

To form the template surfactant cylindrical micelles will self-assemble into a supramolecular aggregate. The size of the aggregate depends on their colloidal stability that relies on the balance of attractive and repulsive interactions with the surrounding medium. When the pH of the medium increases, the generated OH$^-$ groups will interact with the positive charges on the micelle surface, reducing their stability. If the colloidal stability is low, the micelles will aggregate more to reduce the surface energy, forming a larger supramolecular aggregate.[13] The silicon source monomers when added to the system get hydrolysed producing SiOH groups at different rates depending on the base concentration.[13,17,20] At high pH a larger number of these groups are deprotonated (negatively charged) and ready to interact with the positive charged micelles, through strong electrostatic interactions allowing the surfactant-silicates composites to form and exist without the dissolution of the silicates at pH greater than 10.5 (value that is most used in the synthesis of MSNs).[12,13,17,20] The final diameter of the particles will be defined by the size of the supramolecular aggregate (less stable micelles tend to aggregate more, forming larger particles), since the structure of the supramolecular aggregate is frozen once the silica formation starts. Finally, hydrolysis and condensation of the silica precursors occur around the surfactant micelles, leading to the formation of a silica network (**Figure 6**).[13,17,25]
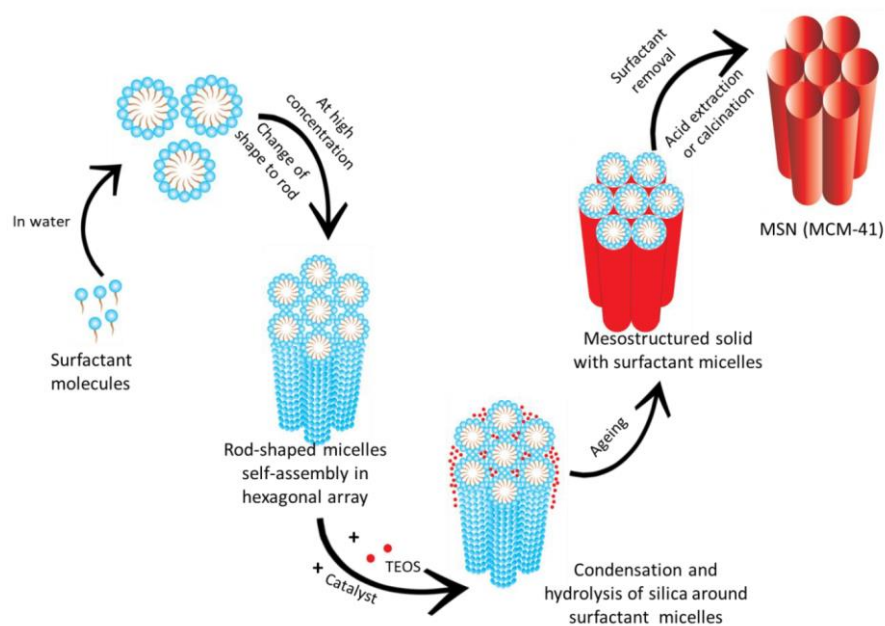
Figure 6. *Mechanism of formation of MCM-41- type mesoporous silica nanoparticles. Adapted from 12.*

As mentioned above, the pH (base concentration) is the most important factor and the one that best defines the particle size. By changing this factor, a good control of particle diameter can be achieved. Maintaining the pH at lower values and increasing the ionic strength is another strategy to control the particle size. The increase in ionic strength leads to a higher screening of the surface charge, that decreases the stability of the micelles, resulting in a formation of larger particles. The surfactant and silica precursor concentrations can also affect the balance between the supramolecular assembly process and the hydrolysis and condensation kinetics of silica formation, ultimately affecting the final size.[25,29]

The reaction parameters can affect not only the size of the particle, but also the mesostructure (hexagonal, cubic, lamellar, etc), the dispersion, the morphology (spheres, fibers, tubules, etc), and the pore size.[17] During this process, aggregation of surfactant-silica nanoparticles must be avoid to obtain a good suspension of MSNs. In order to reduce particle aggregation, dilute conditions must be used (high water/silica precursor and high water/surfactant ratios) to increase the interparticle distance.[17,20] Nanoparticles with a disordered mesostructure were synthesized using a higher amount of silica source, whereas less amount was not sufficient to produce the mesoporous structure.[12,17] The concentration of surfactant also proved to be an important factor in the construction of the mesoporous structure: low concentration of surfactant is not enough to form micelles, affecting formation of the template, while high concentration may result in a disordered structure. The type of surfactant is also crucial to determine

the pore size: surfactants with longer chain length give MSNs with larger pores and those with smaller lengths originate smaller pores.[12]

The last step for the formation of MSNs consists in the removal of the template created by the surfactant micelles, as shown in **Figure 6**. The most used methods to proceed with the extraction are calcination or solvent-extraction[24]. Calcination can be done under air atmosphere at temperatures near 500ºC (dry calcination), resulting in the complete removal of surfactants and the consolidation of the silicate framework via thermal condensation.[16,30,31] Although calcination is a simple and effective method, removal by solvent-extraction is preferred over calcination, since it allows the preservation of the silanol groups and the preservation of the initial porous structure without a significant shrinkage of pores. Typically, a solution of acidified ethanol is employed to remove the template, since the acid will protonate the SiO⁻ groups, destroying the electrostatic interactions between the template and the silica species. This method involves a purification step by multistep centrifugation and redispersion in ethanol, which is considered a drawback because the process takes more time and still does not guarantee the complete removal of the surfactant.[10,16,30] Some other methods have also been suggested, such as dialysis that avoids centrifugation and retains colloidal stability of the suspension, or removal with H_2O_2 that allows the destruction of organic parts found in functionalized mesoporous nanoparticles.[16,32]

The ability to functionalize MSNs can generate a variety of multifunctional particles with versatile applications in different areas. These particles can be selectively functionalized in multiple places, within the silica network, on the outer surface and on the inner surface (inside the pores). The inclusion of molecules or atoms into the silica framework is accomplished by including a silica precursor in addition to the silicon ester during particle preparation, which can serve, for example, to prepare fluorescent MSNs. To obtain a better control over the host–guest interactions with the molecules that are intended to be transported or conjugated to the surface, it is possible to use a post-synthesis treatment to functionalize the surfaces of MSNs through the formation of covalent bonds between the functional groups and the silanol groups that are present in the inner and outer surfaces of these particles. Before extracting the template, it is possible to functionalize the external surface of the particles selectively with molecules capable of interacting with the physiological environment in a coordinated way, counting on a variety of functional groups that can be incorporated on the surface of the particles to bioconjugate proteins, DNA, small molecules, etc (**Figure 7**).[13,33]

The vast variety of applications of MSNs already mentioned in this work is due in part to their ability to accommodate different cargos, as exemplified in **Figure 7**. The surface functionalization of these particles can be used to insert gatekeepers to regulate the encapsulation and release of the cargo loaded inside the pores. After template removal, pores can be functionalized with charged or neutral groups to obtain better control over drug loading and release at the target site as well as to allow molecules that do not interact well with the hydrophilic mesoporous silica to penetrate inside the pores.[12,13,33]
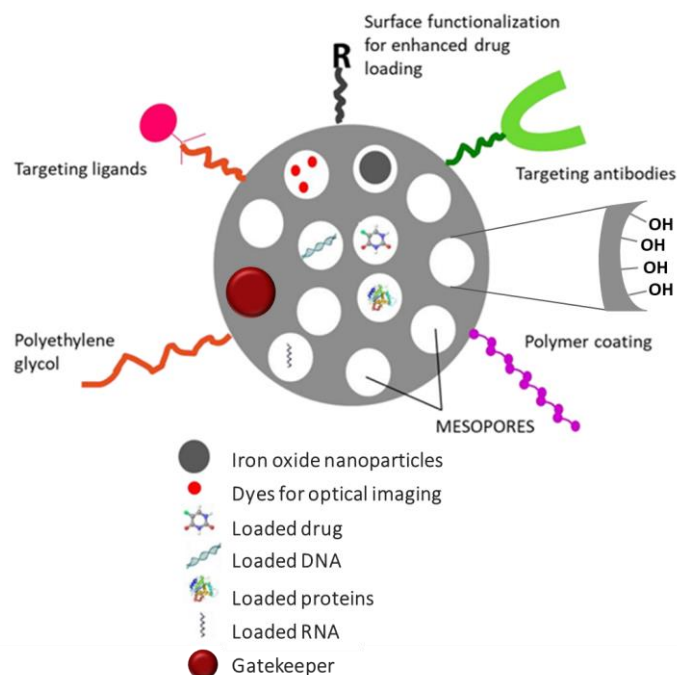
Figure 7. *Schematic illustration to highlight the versatility of MSNs as carriers. Adapted from 12.*

1.2.2. Dual pore Mesoporous Silica Nanoparticles

The possibility of creating silica nanoparticles with two types of pores that can interact independently with two different cargo seems attractive for applications in catalysis, sorption, separation, and biomedical fields.[34] Ideally, this system should be obtained using two different surfactants that do not interfere with each other forming mixed micelles and that could be removed selectively allowing pore functionalization and selective control release.[35]

It is possible to find in the literature some attempts to develop silica nanoparticles containing two different types of pores in their structure. Sun et al.[36] develop a new strategy were a primary mesoporous material of MCM-41 type was produced using CTAB as surfactant to form the template (removed by calcination). This product was crosslinked by condensation of the hydroxy groups located at the surface of the particles with micelles of a triblock copolymer (secondary template) to form the final product which had a bimodal pore distribution. In a more recent paper the same authors illustrate various ways to tune the size and distribution of the secondary nanopores.[37]

Niu et al.[34] also used CTAB, this time combined with amphiphilic block copolymer polystyrene-b-poly (acrylic acid) (PS-b-PAA) to develop a simple method to synthesize dual-mesoporous silica spheres with larger pores in the core and smaller pores in the shell. After the removal of both templates through calcination, core-shell structured dual-mesoporous silica spheres were synthesized.

Another attempt was made by Zhang et al.[38] using CTAB and an ionic liquid (butylamine acetate) as templates to produce in a one-step approach core-shell structured mesoporous silica spheres which were composed of smaller mesopores in the shell and larger mesopores in the core. The same authors proposed a similar strategy but using an alkoxysilyl-functionalized ionic liquid (IL) with organic silicon chain, 1-methyl-3-[3-(trimethoxysilyl) propyl] imidazolium chloride, instead of butylamine acetate, to be employed simultaneously as template and source of silica. The mesopores in the shell and core are generated by CTAB micelles and ionic liquid micelles, respectively. Both templates were removed by calcination to obtain the final particles.[38,39]The mechanism to obtain the desired structure is described in **Figure 8**.
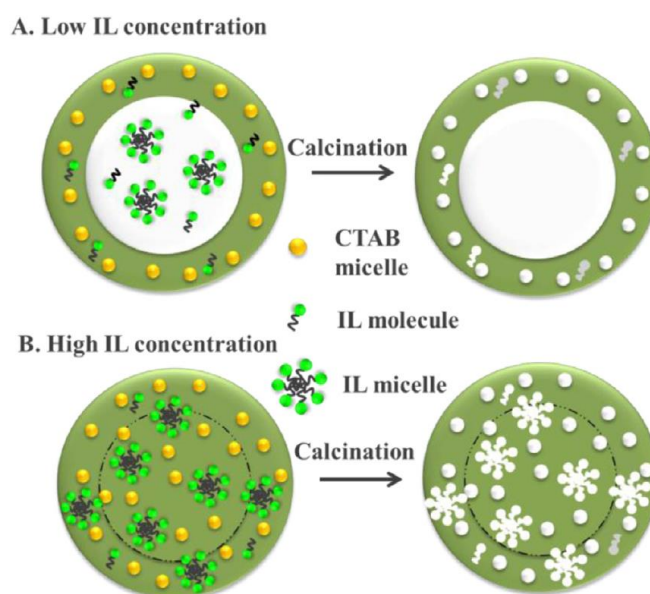
***Figure 8.** Proposed mechanism to obtain core-shell mesoporous silica spheres, using CTAB and an ionic liquid (IL) as templates. Adapted from 38.*

Wang et al.[40] developed dual pore organosilica nanoparticles using lauryl sulfate betaine (LSB) and sodium dodecyl sulfate (SDS) as templates. A single-mesoporous structure was converted into a dual-mesoporous structure by adding larger volume fractions of ethanol to the reaction system, as illustrated in **Figure 9**. The dual-mesoporous particles had an inner core with large mesopores with a flower-like structure, and the outer shell had small mesopores radially orienting from the centre to the external surface.
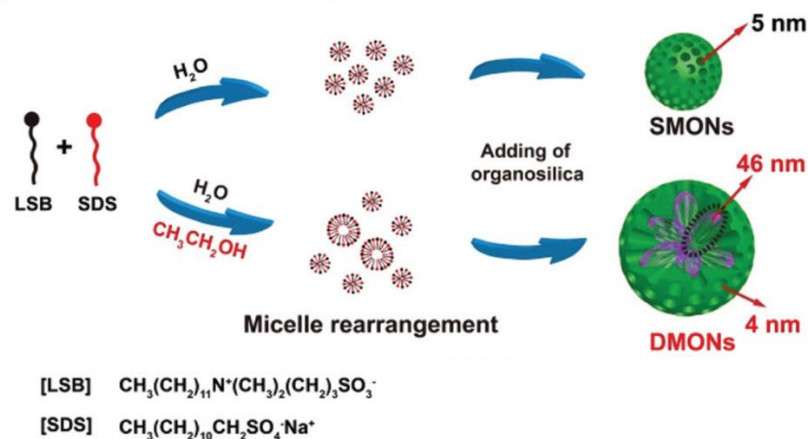
Figure 9. Proposed mechanism for the formation of single-mesoporous organosilica nanoparticles and dual-mesoporous organosilica nanoparticles. Adapted from 34.

Lee et al.[41] synthesized hybrid porous silica nanoparticle containing a dual-sized pore (DpSN) with coexistence of large (40–45 nm) and small (2–3 nm) pores in their core and branch domain with distinctive surface functional groups for multiple strategic cargo loading. Porous silica nanoparticles acting as supporting core for hybrid nanoparticle preparation were synthesized by previously established Stöber method with small modification. DpSN was synthesized by Volmer–Weber growth using aminated SpSN (single pore silica nanoparticles) as template. Park et al.[42] produced silica particles with a non-porous core, an inner shell synthesized on the surface of initial silica nanoparticles with a smaller mesopore (pore size < ~2.5 nm) and an outer shell with a larger mesopore (pore size > ~2.5 nm), as represented in **Figure 10**.
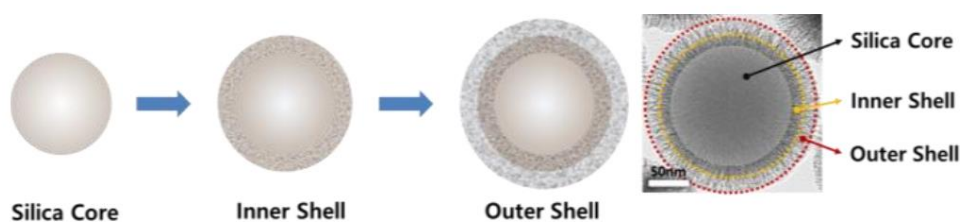
Figure 10. Representative figure of mesoporous silica nanoparticles with double-shells. Adapted from 42.

Recently, Qin et al.[43] developed silica nanospheres with tunable pore sizes (10–30 nm) and hierarchies (dual pores and tri-modal pores), which were synthesized using a new method named hydrophobicity-induced electrostatic interfacial self-assembly (HEISA). To obtain their pore structure the authors used as templates amphiphilic block copolymer polystyrene-block-poly (acrylic acid) (PS-b-PAA), cationic surfactant CTAB and hydrophobic homopolymer polystyrene (PS), that can act as pore-

swelling agent for the enlargement of pore channels and induce the transition from dual-modal to tri-modal pores. After calcination, this tri-modal pore structured silica nanospheres are composed of small mesopores (~2–3 nm) in the silica framework, large mesopores (15–30 nm) in the shells and macropores or voids (> 50 nm) in the cores.

Although these works developed silica nanoparticles with two different pores morphology, in all cases the templates used for the formation of the mesoporous structures were removed by calcination. As mentioned above, calcination is a general method used to remove the template. This method removes all the surfactant organic molecules making it unsuitable to remove selectively the templates and thus selective pore functionalization is impractical, which limits the applications of these materials.

To overcome this problem, an attempt to develop mesoporous silica nanoparticles with a dual pore system with the possibility of selective functionalization was devised by Canadas et al.[14] The strategy consists in using two surfactants (CTAB and HFDePC (1H1H2H2H-perfluorodecylpyridinium chloride)) as templates and selectively remove them by extraction using organic solvents. This extraction process proved to be inefficient to remove selectively the templates, leaving the issue open for other strategies to successfully produce the desired mesoporous nanoparticles with a dual pore system. To achieve that a two-surfactant system must be design to allow selective removal of one template and to allow selective functionalization.[14]

1.3. Templates

One possible alternative may rely on the use two surfactants where one of them can be selectively removed through a controlled stimulus (stimuli responsive surfactant), as represented in **Figure 11**. Cleavable surfactants contain a bond that has intentionally been introduce between the hydrophilic part and the hydrophobic part and breaks down in a controlled way using a stimulus.[44] The cleavage of this bond will lead to one water-soluble and one water-insoluble product that can usually be removed by standard workup procedures, which is interesting for surfactants employed in numerous biochemical applications.[45]
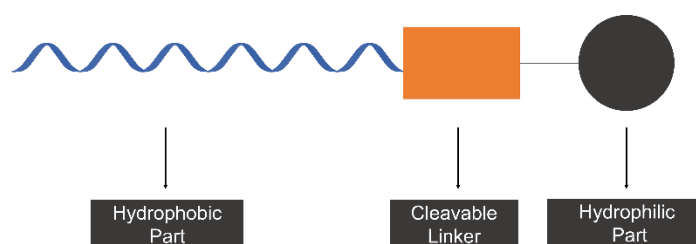
Figure 11. *Structure of a stimuli responsive surfactant, containing a hydrophilic part, a cleavable linker, and a hydrophobic part.*

1.3.1. Stimuli Responsive Surfactants

Several surfactants were designed taking advantage of a specific stimulus (stimuli responsive surfactants). Stimuli are commonly classified in three categories: physical (light, temperature, ultrasound, magnetic, mechanical, electrical), chemical (solvent, ionic strength, electrochemical, pH), or biological (enzymes, receptors).[44,46]

To design a stimuli responsive surfactant some basic requirements must be taken into consideration: simple synthesis, surface activities comparable to those of non-functional surfactants, high stability before and during their use, high and controlled cleavability, etc.[47] These factors were taken into consideration by several authors that designed new structures to obtain cleavable surfactants that respond efficiently to a stimulus.

A photolabile surfactant containing a α-methyl-*o*-nitroveratryl (ONV) group as linker was design by Hwang et al.[32] This group was placed between the hydrophilic and the hydrophobic parts with different alkyl chain lengths (8, 10, and 12 carbons), as described in **Figure 12**. ONV-C12 surfactant formed irregular-shaped spherical structures, suggesting micelle structures. ONV-C10 surfactant molecules formed vesicular structures and ONV-C8 surfactant failed to form any supramolecular structure. After

irradiation with a light source of 365 nm, the link between the polar group and the ONV group was cleaved (as shown in **Figure 12**) leading to the disassemble of the supramolecular structures.
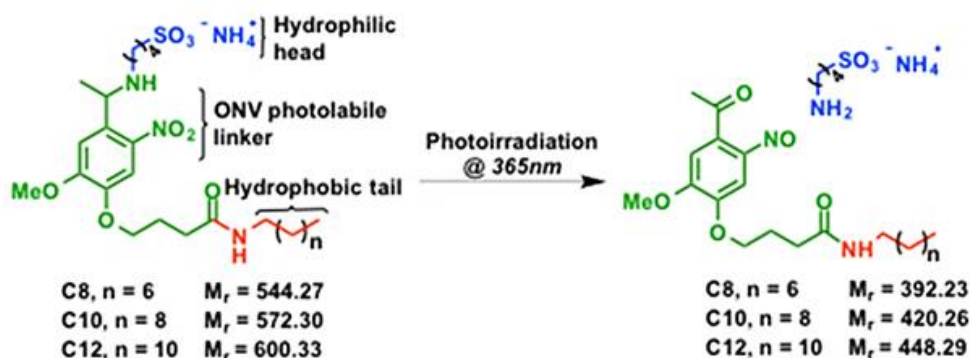
Figure 12. Representation of the structure of surfactants containing an ONV photolabile linker. After irradiation with a light source of 365 nm the ONV group is cleaved. Adapted from 32.

Another type of cleavable surfactant has designed by Thyaumanavan et al.[48] taking advantage of disulfide chemistry. A disulfide bond was placed between the hydrophilic group and the hydrophobic part, as represented in **Figure 13**. SA-1 and SA-2 formed mixed micellar aggregates that were dissembled using dithiothreitol (DTT), responsible for the cleavage of the disulfide bond.
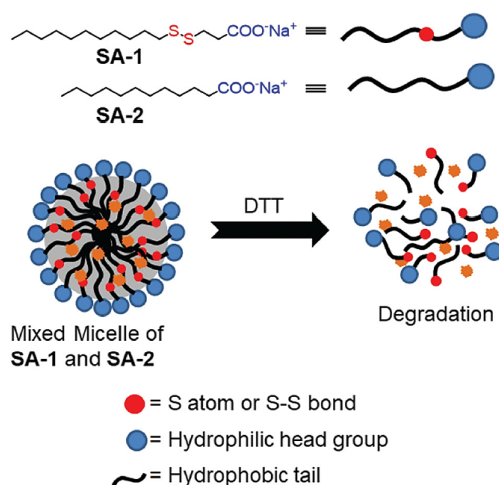
Figure 13. Representation of micelle disassembly after cleavage with DTT of surfactants containing a disulfide bond (SA-1 and SA-2). Adapted from 49.

Surfactants that contain a thermally labile bond as linker have been prepared by a Diels-Alder addition reaction (**Figure 14**). The reaction involves the cycloaddition between a diene and a dienophile. When exposed to high temperatures, the retro Diels-Alder reaction occurs, and the surfactant is decomposed into its parts with the loss of surface activity, thereby destroying the surfactant structure through a non-invasive process.[47]
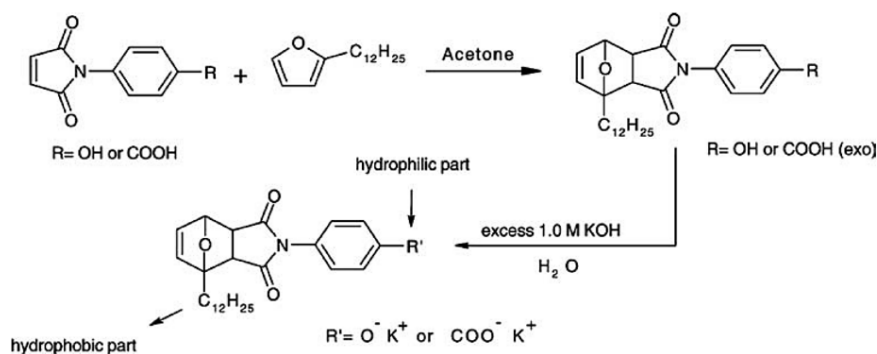
Figure 14. *Synthesis of a cleavable surfactant by Diels-Alder reaction. Adapted from 47.*

1.3.2. Cleavable Functional Groups

Among the variety of stimuli that can be applied, the most common are temperature, pH, light, or redox environment. Examples of functional groups related to each of these stimuli are presented in **Table 1**.

Table 1. *Examples of cleavable functional groups and the respective stimuli responsible for their breakdown.*

Stimulus		Functional Group	Reference
Temperature			47
pH	Basic		50
	Acidic		51
Light			52
Redox environment			49

16

Thermolabile groups have advantage over chemically cleavable groups, since the transfer of heat is more evenly distributed throughout the MSNs as heat does not need to penetrate the pore like chemicals do.[53] The Diels-Alder reaction can be used to produce thermolabile groups efficiently, as mentioned earlier.[47] Temperature is a key parameter in the synthesis of MSNs therefore it must be changed carefully. Temperatures above 40 ⁰C should be used, since the photolabile group needs to remain intact during the synthesis. The use of temperatures around 80 ⁰C represents a problem because it can lead to the removal of both surfactants.

Chemical hydrolysis of surfactants is performed using acidic or basic conditions depending on the linker placed between the polar group and the hydrophobic group. Esters are very labile when subjected to alkaline conditions, making them a suitable choice as the alkali-sensitive group in surfactants. An example of a cleavable surfactant containing an ester linkage is shown in **Table 1**, taken from reference [50]. Other groups like amides or carbonates can also be used. On the other hand, the majority of acid-labile surfactants contain an acetal group, as exemplified in **Table 1**.[45,51] pH is a stimulus difficult to apply in the case of MSNs synthesis, since the target group must resist to basic conditions (synthesis conditions) and low pH cannot be applied because silica species will become protonated destroying the interaction between silicates and micelles of both surfactants, leading to the simultaneous removal of the two templates, leaving all pores free, and discarding the possibility of selective functionalization.

Light as external stimulus can provide some advantages over other stimuli as it allows a non-invasive and controlled trigger with higher spatial resolution.[46] When a photolabile group is added to a surfactant molecule, it can be fragmented using UV irradiation, or undergo conformational isomerization.[32] Groups like azobenzene, spiropyran and cinnamic ester respond to light by reversible isomerization.[54] The most popular photolabile groups are *o*-nitrobenzyl esters (**Table 1**, adapted from reference [52]) and their analogues. When irradiated with UV light these groups undergo a Norrish type II reaction that leads to their cleavage. By introducing specific substituents on the aromatic ring, it is possible to tune the wavelength at which the bond cleavage is possible. Another advantage of these groups compared with other photolabile groups is their reduced steric hindrance, which is important to guarantee an adequate critical packing parameter for the formation of cylindrical micelles.[55]

Disulfide groups induce redox responsiveness when exposed to a reducing environment, resulting in their cleavage with the formation of two thiol groups. In the presence of glutathione, or its smaller analogues (e.g., dithiothreitol (DTT) or mercaptoethanol), disulfide bonds undergo bond cleavage. An example of a surfactant containing a disulfide bond taken from reference [49] is presented in **Table 1.** A disulfide bond placed between the polar group and the hydrophobic group of a surfactant, in the presence of a reducing environment, leads to the separation of the surfactant molecule into two parts.[46,49]

1.3.3. Smart surfactants for dual pore MSNs synthesis

Smart surfactants or stimuli responsive surfactants could be easily introduced as templates for the synthesis of dual pore system MSNs with selective functionalization/loading, although such approach is not reported in the literature. To synthesize the dual pore system MSNs with selective functionalization/loading, a two-surfactant system would be employed, consisting in a non-cleavable surfactant (inert surfactant) and a smart surfactant (cleavable) that could be selectively removed, as represented in **Figure 15**.

This smart system relies on the preparation of MSNs using two templates and their selective removal. A critical point that must be avoided is the formation of mixed micelles between both surfactants. After synthesis, the smart surfactant is removed (using the appropriate stimuli), and it is possible to functionalize the free pores or load it with a specific cargo. Afterwards, the second template can be removed by solvent extraction (with an acidified ethanol solution) and the resulting free pores can be functionalized or loaded with a second cargo, enabling the transport of two distinct cargos in the same particle (**Figure 15**).
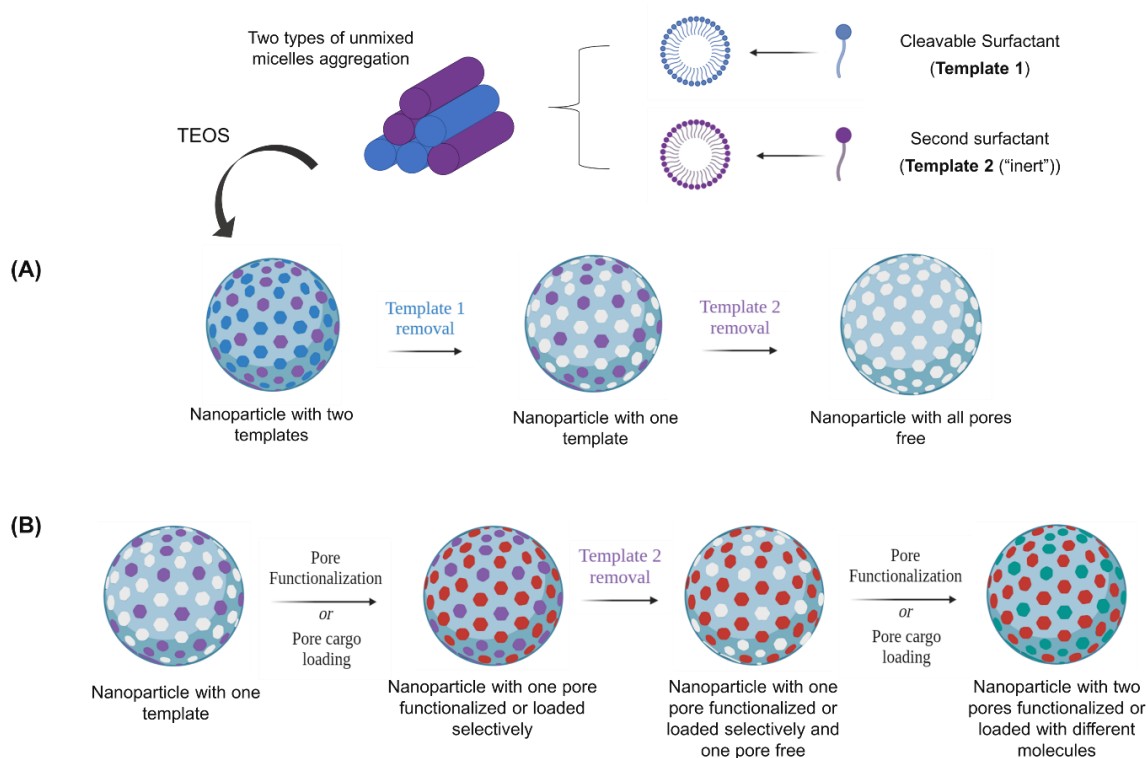
Figure 15. *Schematic representation of the strategy devised to produce a dual pore system MSN. A two-surfactant system containing a smart surfactant and a non-cleavable surfactant was designed to produce the dual-mesoporous structure enabling the selective removal of the templates **(A)**. After the selective removal of each template the resulting free pores can be selective functionalized or loaded with different cargos **(B)**.*

1.4. Objectives and Work Strategy

The goal of this project is to synthesize a smart surfactant with a cleavable group, that upon stimulus application suffers an irreversible structural change, yielding non-amphiphilic moieties. This smart surfactant should have a critical packing parameter (cpp) between 0.33-0.5 (to form cylindrical micelles) and be stable under MSNs synthesis conditions (pH 9-11 and temperature close to 40ºC).

The structure of the smart surfactant must comprise a linker between the polar (cationic) and hydrophobic parts. The selection of the linker group is closely related to the stimulus used to disrupt the surfactant structure, since the stimulus will have to be selective, namely, disturbing only the smart surfactant and leaving intact the structure of the particles and other surfactants.

Two surfactant structures (**Figure 16**) were planned, based on the possible use of different stimulus. Both structures A and B were designed to be structurally similar to cetyltrimethylammonium bromide (CTAB), which is commonly used as template for MSNs synthesis: the polar group is a quaternary amine, and the hydrophobic group is defined to have the same number of atoms as the hydrophobic part of CTAB.

Structure A is a light responsive surfactant that contains a *o*-nitrobenzyl ether group as linker between the hydrophilic and hydrophobic parts. This group was chosen instead of its ester analogue (represented in **Table 1**) due to the possibility of the later undergoing hydrolysis when subjected to basic pH during MSN synthesis. Structure B is represented a redox responsive surfactant, containing a disulfide bond as linker to take advantage of its reactivity in the presence of a reducing agent, such as dithiothreitol (DDT) or its analogues.

Finally, the behavior of the two molecules in solution was tested to find the best template to combine with an inert surfactant, for the synthesis of dual pore MSNs.

(A)

(B)
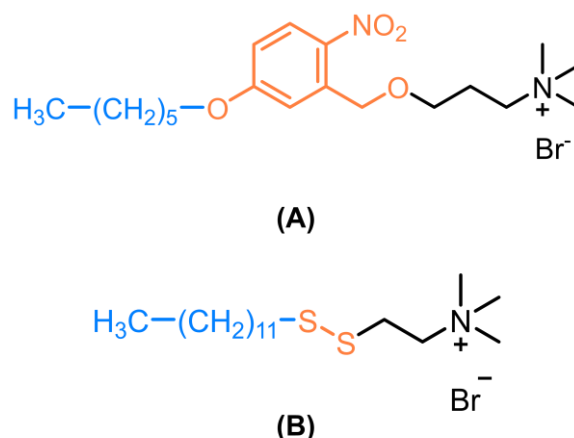
Figure 16. *Two possible structures for the cationic (containing a quaternary ammonium polar group) cleavable surfactant containing (**A**) a light responsive group (light penetrates easily inside the pores) and (**B**) a redox responsive group (cleaved by DTT, a small molecule) as linkers. Both structures guarantee the stability of the surfactant during the MSNs synthesis and the selective removal of the cleavable surfactant through a specific stimulus. These surfactants should form cylindrical micelles and avoid the formation of mixed micelles with the second surfactant.*

2. Experimental Part

2.1. Materials

All reagents and solvents were purchased from commercial suppliers without further purification except for dimethylformamide and tetrahydrofuran that were dried over molecular sieves. The following materials were used without further purification: iodomethane (≥99.0 %, Sigma-Aldrich), sodium hydride (dry, 90%, NaH, Sigma-Aldrich), (3-bromopropyl)trimethylammonium bromide (97%, Sigma-Aldrich), 1-Dodecanethiol (≥98%, Sigma-Aldrich), 1-bromohexane (≥98%, Sigma-Aldrich), 5-hydroxy-2-nitrobenzyl alcohol (97%, Sigma-Aldrich), cesium carbonate (99% Cs_2CO_3, Sigma-Aldrich), potassium carbonate (Sigma-Aldrich, ≥99%) , 2-dimethylaminoethanethiol hydrochloride (95%, Sigma-Aldrich), Amberlite IRA-410 chloride form (Sigma-Aldrich), sodium hydroxide (Pure NaOH, PanReac AppliChem), tetrahydrofuran (ACS reagent, THF, Carlo Erb a Reagents), Dithiothreitol (97%, Sigma-Aldrich), methanol (Fisher Scientific, MeOH, ≥99.8%), ethyl acetate (Fisher Scientific, EtOAc, ≥99.8%), dimethylformamide (Fisher Scientific, DMF, ≥99.8%), acetonitrile (Fisher Scientific, MeCN, ≥99.8%) and dichloromethane (99.95% DCM, José Manuel Gomes dos Santos, Lda). The deionized (DI) water was generated using a Millipore Milli-Q system (≥18 MΩcm, Merck, NJ, USA). PLC silica gel 60 F_{254} plates were purchase in Sigma-Aldrich.

Evolution of reactions was followed by thin-layer chromatography (TLC) using silica gel 60 F_{254} Aluminium plates and revealed by UV light at 254 nm and 325 nm and, when needed, in an iodine chamber.

2.2. Equipment

2.2.1. Nuclear magnetic resonance spectroscopy (NMR)

^{1}H NMR, ^{13}C NMR and ^{1}H -^{13}C HSQC spectra were acquired on a Bruker Avance III 400 (at 400.13 and 100.613 MHz) spectrometer. Deuterated solvents such as $CDCl_3$, MeOD and DMSO-d_6 were used. Chemical shifts (δ) and coupling constants (J) are expressed in ppm and in Hertz (Hz), respectively.

2.2.2. Mass spectrometry

ESI mass spectra were recorded on a LCQ Fleet mass spectrometer with an ESI source (Thermo Scientific) interfaced with an HPLC-DAD (Varian).

2.2.3. ATR-FTIR spectroscopy

ATR-FTIR spectra were recorded in the range of 4000–400 cm^{-1} on an Agilent Cary 630 FTIR spectrometer (Agilent Technologies).

2.2.4. Raman spectroscopy

Raman spectra (Labram HR 800 Evolution, Horiba JobinYvon) was obtained with 532 and 633 nm excitation with a 600 grove/mm grating; laser power at the samples was ~10 mW and the unpolarized data were collected for 10s and 60s and 4 scans and 1 scan, at room temperature, using a 100x objective lens. CTAC-SS spectra was obtained with two different excitation wavelengths because the compound showed fluorescence when excited at 523 nm, thus the compound was excited at 633 nm from 1600 cm^{-1} to 3000 cm^{-1}.

2.2.5. UV-Vis Spectroscopy

A Jasco V-660 UV-VIS Spectrophotometer (Oklahoma City, OK, USA) with a double monochromator and photomultiplier tube detector for higher resolution was used to record the absorption spectra. The measurements were carried out in 10 mm quartz cells at room temperature.

2.2.6. Surface Tension Measurements

Attention Theta optical tensiometer (Biolin Scientific, Sweden) was used to measure the surface tension of CTAC-SS solutions and the results were analysed using OneAttension software (Nanoscience Instruments, Phoenix, USA). The main components of the optical tensiometer are a camera, dispenser to dispense a drop, sample stage, and the light source to illuminate the drop on the sample stage.

2.2.7. Dynamic Light Scattering (DLS)

Zetasizer Nano ZS (Malvern Instruments, UK), model ZEN3600, with 173º and 90º detector was used to determine the hydrodynamic diameters of the particles in solution, assuming Brownian movement.

2.3. Methods

2.3.1. Synthesis of novel stimuli responsive surfactants

2.3.1.1. Compound **1**

A mixture of 5-hydroxy-2-nitrobenzyl alcohol (300 mg, 1.77 mmol) and K_2CO_3 (735 mg, 5.31 mmol, 3 eq) was stirred in dry DMF (8 mL), for 1h at 60 °C under argon atmosphere. Bromohexane (0.37 mL, 2.655 mmol, 1.5 eq) was added dropwise to the reaction mixture and stirred for 3h at 60 °C under argon atmosphere. The reaction was monitored by TLC using hexane: EtOAc (2:1) as eluent. DMF was removed under reduced pressure. The resulting residue was dissolved in ethyl acetate and washed three times with water and brine. The organic phase was dried over $NaSO_4$, filtered, and evaporated under vacuum. The resulting product was obtained as a yellow-brown oil (440.6 mg, 98% yield). **^{1}H NMR** (400 MHz, $CDCl_3$) δ 8.19 (d, J = 9.1 Hz, 1H), 7.22 (d, J = 2.4 Hz, 1H), 6.89 (dd, J = 9.1, 2.6 Hz, 1H), 5.00 (s, 2H), 4.09 (t, J = 6.5 Hz, 2H), 1.87 – 1.80 (m, 2H), 1.52 – 1.45 (m, 2H), 1.38 – 1.36 (m, 4H), 0.93 (t, J = 6.8 Hz, 3H).**^{13}C NMR** (100 MHz, $CDCl_3$) δ 163.9, 140.2, 140.1, 128.1, 114.8, 113.6, 68.9, 63.1, 31.5, 28.9, 25.6, 22.6, 14.0.

2.3.1.2. Compound **2**

Compound **1** was dissolved in dry DMF, at 0 °C under argon atmosphere. Dry NaH was added portion-wise to the stirring reaction and after 10 minutes (3-bromopropyl)trimethylammonium bromide (TAB) was added gradually to the reaction mixture and left to react for 1h at 0 °C and at least 1h at room temperature. The reaction was monitored by TLC using hexane: EtOAc (3:1) as eluent. The reaction was quenched with water and the aqueous phase was washed with EtOAc three times. The organic phases were combined and washed with a saturated Na_2CO_3 solution, brine and dried over anhydrous sodium bicarbonate. The reaction crude was purified by Preparative TLC plates using hexane: EtOAc (3:1) as eluent. Fractions from the preparative plate were scraped and the content of each fraction was extracted using organic solvents.

Several changes were made to this protocol resulting in six attempts to synthesize compound **2**. **Table 2** describes the conditions changed in each attempt, and observations related to the synthetic procedure.

Table 2. *Description of the procedure optimization performed to the general protocol in the attempt to obtain compound **2**, along with general observations related to the synthetic procedure.*

Reactions	Conditions	Observations
Attempt 1	NaH (2.4 eq) TAB (1.1 eq)	Three fractions were removed and analysed by NMR.
Attempt 2	NaH (2.2 eq) TAB (2.3 eq)	
Attempt 3	NaH (2.2eq + 1.2 eq after 3h) TAB (2.3 eq + 0.5 eq after 3h)	
Attempt 4	NaH (2.2 eq) TAB (2.3 eq)	NaH used was dispersed in mineral oil. Resulting crude washed with hexane to try to obtain the desired compound and remove the starting material.
Attempt 5	NaH (2.2 eq) TAB (2.3 eq)	NaH in excess was washed previously with hexane in a round bottom flask and stirred for 15 minutes. The solvent was carefully removed and NaH was ready to use.
Attempt 6	NaH (2.2 eq) TAB (2.3 eq)	NaH used was dry and recently opened.

Attempt 1: Three fractions were removed from the Preparative TLC plate after elution: Fraction 1 (F1), Fraction 2 (F2) and Fraction 3 (F3), in decreasing order of retention coefficient. **F1**: ^{1}**H NMR** (400 MHz, CDCl$_3$) δ 10.51 (s, 1H), 8.18 (d, J = 9.1 Hz, 1H), 7.33 (d, J = 2.6 Hz, 1H, 7.15 (dd, J = 9.0, 2.5 Hz, 1H), 4.12 (t, J = 6.5 Hz, 2H), 1.89 – 1.82 (m, 3H), 1.53 – 1.46 (m, 3H), 1.37 (m, J = 3.3 Hz, 6H), 0.93 (d, J = 6.6 Hz, 5H). **F2:** ^{1}**H NMR** (400 MHz, CDCl$_3$) δ 8.20 (d, J = 9.1 Hz, 1H), 7.22 (s, 1H), 6.90 (d, J = 9.1 Hz, 1H), 5.00 (s, 2H), 4.09 (t, J = 6.3 Hz, 2H), 1.88 – 1.82 (m, J = 14.3, 6.2 Hz, 2H), 1.49 (s, 2H), 1.37 (s, 4H), 0.94 (s, 3H).

Attempt 3: ^{1}**H NMR** (400 MHz, DMSO-d$_6$) δ 8.13 (d, J = 9.1 Hz, 1H), 7.33 (d, J = 2.6 Hz, 1H), 7.02 (dd, J = 9.1, 2.8 Hz, 1H), 4.85 (s, 2H), 4.11 (t, J = 6.5 Hz, 2H), 1.78 – 1.71 (m, 2H), 1.46 – 1.39 (m, 2H), 1.33 – 1.30 (m, 4H), 0.88 (t, J = 6.9 Hz, 3H).

2.3.1.3. Compound 3

2-(dimethylamino)ethanethiol hydrochloride (100 mg, 0.7059 mmol), 1-dodecanethiol (0.19 mL, 0.77649 mmol, 1.1 eq), Cs_2CO_3 (92 mg, 0.21177 mmol, 40 mol%) and CH_3CN (4 mL) were added to a 25 mL round bottom flask and the mixture was stirred under air at 60°C for 24 h. The reaction was monitored by TLC using dichloromethane/ methanol 5% as eluent. After cooling to room temperature, the solvent was evaporated under reduced pressure. Water was added (10 mL) to the resulting residue and the pH was increased until 8 by adding drops of a NaOH solution (0.5 M). The solution was washed with ethyl acetate two times. The organic phases were combined, dried over $NaSO_4$, filtered, and evaporated under vacuum.

The reaction crude was purified by Preparative TLC plates (dichloromethane/ methanol 5%) to give the desired product. The silica from the plates was scraped from the area corresponding to the stain of the desired product. The silica was placed on a Soxhlet, and the product extracted using ethyl acetate for 24h. The solvent was evaporated under reduced pressure to obtain the desired product (118.1 mg, 55% yield). **¹H NMR** (400 MHz, $CDCl_3$) δ 2.82 (t, J = 7.9 Hz 2H), 2.71 (t, J = 7.1 Hz, 2H), 2.63 (t, J = 7.1 Hz, 2H), 2.29 (s, 6H), 1.72-1.65 (m, 2H), 1.41 – 1.27 (m, 18H), 0.89 (t, J = 6.7 Hz, 3H). **¹H NMR** (400 MHz, MeOD) δ 2.82 (t, J = 7.7, 2H), 2.75 – 2.67 (m, 4H), 2.31 (s, 6H), 1.74 – 1.67 (m, 2H), 1.48 – 1.31 (m, 20 H), 0.92 (t, J = 6.0 Hz, 3H).**¹³C NMR** (100 MHz, $CDCl_3$) δ 58.8, 45.3, 39.2, 36.7, 31.9, 29.7, 29.7, 29.6, 29.6, 29.5, 29.4, 29.2, 29.2, 28.6, 22.7, 14.1. **ESI⁺-MS** m/z 306.17 (M+H⁺)

2.3.1.4. Compound 4

A mixture of **3** (92.7 mg, 0.0965 mmol), excess of CH_3I and CH_3CN (6 ml) were added to a 25 mL round bottom flask and refluxed for 24 h at 95°C, under argon atmosphere. The solvent and excess of CH_3I were leaved to evaporate overnight inside the fume hood. The remaining solvent was removed in the vacuum line to give the redox sensitive surfactant (117.5 mg, 87% yield) as an orange solid. **¹H NMR** (400 MHz, MeOD) δ 3.78 (t, J = 8.6 Hz, 2H), 3.26 (s, 9H), 2.70 (t, J = 7.2 Hz, 2H), 1.74 – 1.66 (m, 2H), 1.44-1.32 (m, 18H), 0.92 (t, J = 6.6 Hz, 3H). **¹³C NMR** (100 MHz, MeOD) δ 65.3, 52.7, 52.6, 52.6, 38.4, 31.7, 30.6, 29.4, 29.4, 29.3, 29.2, 29.1, 28.9, 28.8, 28.0, 22.3, 13.0. **ESI⁺-MS** m/z 320.14 (M⁺).

Compound **4** counterion was change from iodine to chloride using an ionic exchange resin. 100 mg of compound **4** were added to a round bottom flask and methanol was added until the compound was completely dissolved. 197.12 mg of resin (Amberlite IRA-410 chloride form) were added to the mixture and left to stir for 24 h. The resin was filtered, and the solvent evaporated under pressure to obtain CTAC-SS. **¹H NMR** (400 MHz, MeOD) δ 3.75 (t, J = 8.6 Hz, 4H), 3.24 (s, 20H), 2.71 (t, J = 7.2 Hz, 2H), 1.73 – 1.66 (m, 2H), 1.46 – 1.32 (m, 18H), 0.92 (t, J = 5.9 Hz, 3H). **ESI⁺-MS** m/z 320.14 (M⁺).

2.3.2. Preliminary studies with CTAC-SS

2.3.2.1. Degradation studies for CTAC-SS

To perform the degradation studies, an aqueous solution of 2.5 mM of CTAC-SS and a 10mM aqueous solution of DTT were prepared and 1 mL of each solution was mixed (1.25 mM of CTAC-SS + 5 mM of DTT) in a quartz cuvette and the evolution over time of the absorption spectrum of the mixture was recorded in a Jasco V-660 UV-VIS spectrophotometer.

2.3.2.2. Computational studies

Geometry optimization of the cations of CTAB and CTAC-SS was performed using the electronic structure calculation program Gaussian 09 at the BLYP/6-31G (d,p) level of approximation in vacuum.[59] The calculation of the vibrational frequencies was used to confirm that a minimum in the potential energy surface (PES) was achieved (lack of imaginary frequencies). For both CTAB and CTAC-SS the initial structure for geometry optimization consisted in a planar chain of carbon (or carbon and sulphur) atoms in a zig-zag conformation. The optimized structures were analysed using Avogadro software (https://avogadro.cc/).

2.3.2.3. Determination of the critical micelle concentration (CMC) of CTAC-SS

Surfactants are amphiphilic molecules, meaning they have a hydrophobic part and a hydrophilic part. At low concentrations the surfactant molecules adsorb at the liquid-gas interface, with the hydrophobic part minimizing the contact with water. Upon concentration increase, the interface is occupied by surfactant molecules and at a moment concentration the interface is full. For higher concentrations, the surfactant molecules self-assemble into micelles (hydrophobic part inside and hydrophilic part to the outside) and they are dispersed inside the solution. The critical micelle concentration (CMC) is the concentration where the interface is full and the first micelles are formed. [56]

The surface tension of a surfactant solution is linearly dependent on the logarithm of the concentration for low concentrations values. For concentrations above the CMC the surface tension remains constant with the increase of the concentration. The CMC value can be determined by the intersection of the fittings to the points in the two regimes, as shown in **Figure 17**.[57]
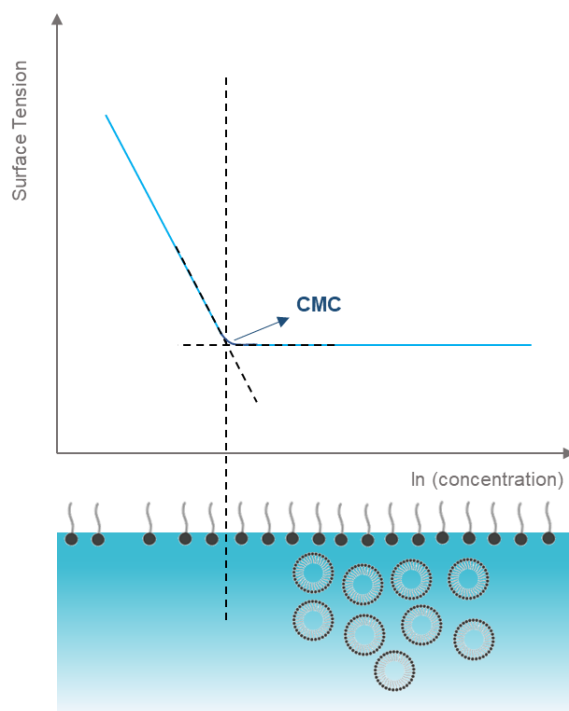
Figure 17. *Schematic plot of the surface tension as a function of the logarithm of the concentration of surfactant.*

The surface tension can be measured using an Optical Tensiometer, that relies on the pendant drop method. The shape of the drop hanging from a pipette tip is determined from the balance of forces which include the surface tension of the liquid being analysed. The surface or interfacial tension can be related to the drop shape, $\gamma = \Delta\rho g R_0/\beta$, where γ is the surface tension, $\Delta\rho$ is the density difference between fluids, g is the gravitational constant, R_0 is the drop radius of curvature at the apex, and β is the shape factor. β can be defined through the Young-Laplace equation expressed as 3 dimensionless first-order equations. [58]

Solutions of CTAC-SS with concentrations ranging from 0.05 to 3.5 mM were prepared in water at pH 7, measured and analysed using OneAttension software. Surface tension was measured 140 times to obtain the mean value and standard deviation for each concentration of CTAC-SS.

3. Results and Discussion

The goal of this work was to develop mesoporous silica nanoparticles with a dual pore system. The strategy to obtain the desired particles involves a two-template system composed of a smart surfactant and an inert surfactant. This project focused on the synthesis of a light responsive surfactant and a redox responsive surfactant that were designed to be employed in the synthesis of dual pore MSNs as the stimuli responsive surfactant, taking into consideration the previously mentioned requirements. Afterwards, the smart surfactants must be evaluated to determine their behavior in solution and responsiveness to the respective stimulus. These results will determinate their potential as templates for the synthesis of the dual pore MSNs.

3.1. Synthesis and characterization of the light responsive surfactant

The desired photocleavable surfactant was prepared following a synthetic route (**Figure 18**) of two steps using as starting material the 5-hydroxy-2-nitrobenzyl alcohol.[60] The addiction of the hydrophobic part to the linker is made in the first step (compound **1**), and in a second step the hydrophilic part is added to the previous compound, resulting in the formation of the final molecule, compound **2**.
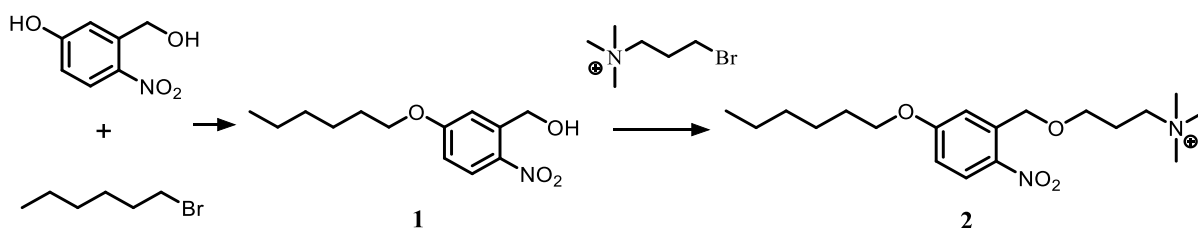
Figure 18. *Scheme for the synthesis of the light sensitive surfactant (compound **2**).*

The first attempt to synthesize compound **1** consisted in a mixture of 5-hydroxy-2-nitrobenzyl alcohol with triethylamine (TEA) that was stirred in dry THF at 0 °C, under inert atmosphere. Triethylamine is a weak base, so it removes only the more labile proton leading to the formation of a phenolate, that will attack 1-bromohexane through a nucleophilic substitution (S_N2) reaction, generating compound **1**. The reaction was followed by TLC and after 18 h no additional spots were identified on the TLC analysis, indicating that the reaction did not take place. It was necessary to search for alternative synthesis conditions, which resulted in the second attempt [61] to synthesize compound **1**, described in **Figure 19**.
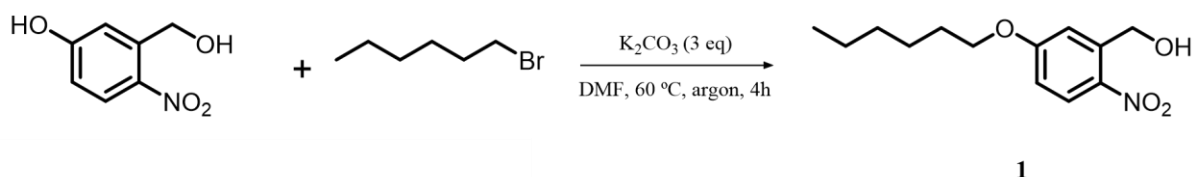
Figure 19. *Scheme for the synthesis of compound **1**.*

In this approach potassium carbonate (K_2CO_3) is used as base and mixed with 5-hydroxy-2-nitrobenzyl alcohol in dry DMF at 60 °C, under inert atmosphere. Bromohexane was added to the reaction mixture and the reaction was monitored by TLC, and after 4h the benzyl substrate was totally consumed. After the workup procedure, compound **1** was obtained as a yellow-brown oil in 98 % yield.

The ^1H NMR spectrum of compound **1** (**Figure 20**) shows three peaks corresponding to the three aromatic protons: two doublets at δ 8.19 (H_{C9}) (J= 9.1 Hz) and 7.22 ppm (H_{C12}) (J= 2.4 Hz) and one doublet of doublets at δ 6.89 ppm (H_{C8}) (J= 9.1, 2.6 Hz). Together with the information from ^1H - ^{13}C HSQC spectrum (**Figure 22**) it was possible to assign the remaining protons to the respective carbons. The singlet located at δ 5 ppm integrates to two protons that are connected to C_{13} and the triplet located at δ 4.09 (J = 6.5 Hz) refers to the two protons linked to C_6. The multiplets integrating to two protons, at δ 1.87 – 1.80 and 1.52 – 1.45 ppm, and the multiplet located at δ 1.38 – 1.36 ppm that integrates to four protons, correspond to protons from the carbons in the alkyl chain. The three protons of C_1 appear as a triplet located at δ 0.93 ppm (J = 6.8 Hz).
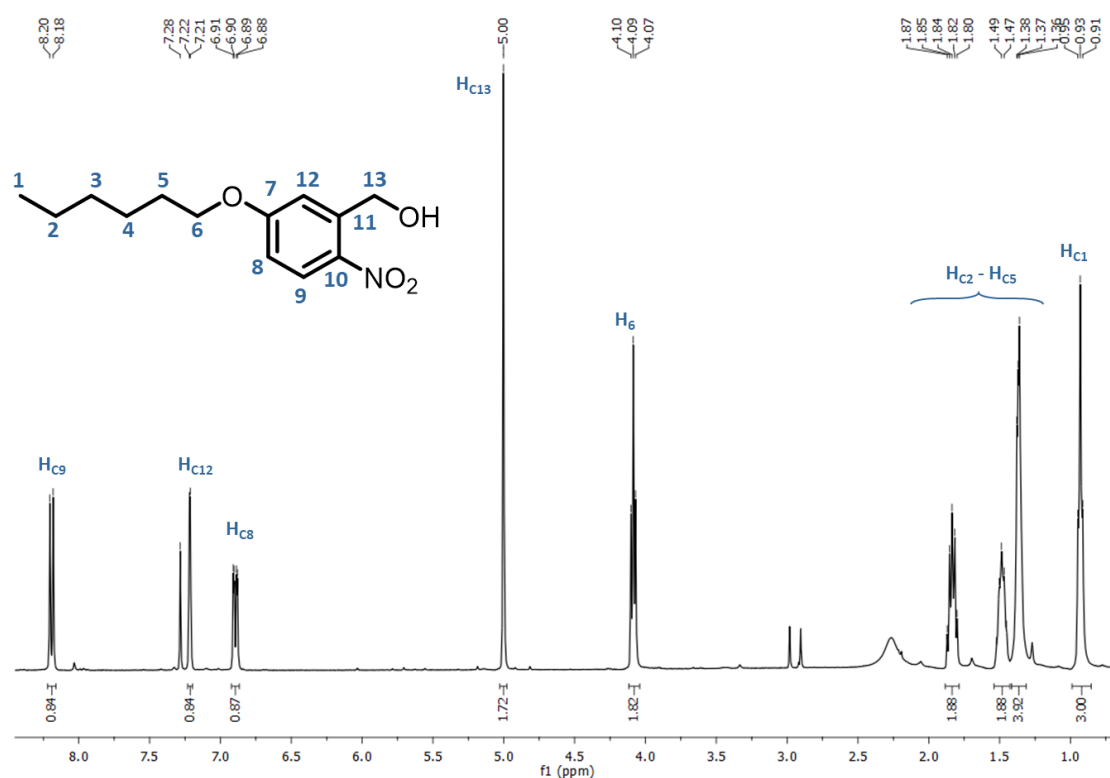
Figure 20. *^1H NMR spectrum of compound **1** in CDCl₃.*

The successful preparation of compound **1** was corroborated by the analysis of ^{13}C NMR **(Figure 21)** and ^1H - ^{13}C HSQC spectra (**Figure 22**). The three quaternary carbons from the aromatic ring, C_7, C_{10} and C_{11}, are related to the peaks located at δ 163.9, 140.2 and 140.1 ppm. The remaining aromatic carbons are located at δ 128.1 (C_9), 114.8 (C_{12}) and 113.6 ppm (C_8). The peak related to carbon C_{13} is

located at δ 63.1 ppm and the carbons from the alkyl chain are associated to signals at δ 68.9 (C_6), 31.5, 28.9, 25.6, 22.6, and 14.0 ppm (C_1).

Compound **1** was analysed by ESI⁺-MS (Figure A.1, Appendix A), with a peak with high intensity appearing at m/z 214.26, but the results did not enable the identification of any compound. This does not imply that the compound was not produced, just means that it cannot be identified using this method.
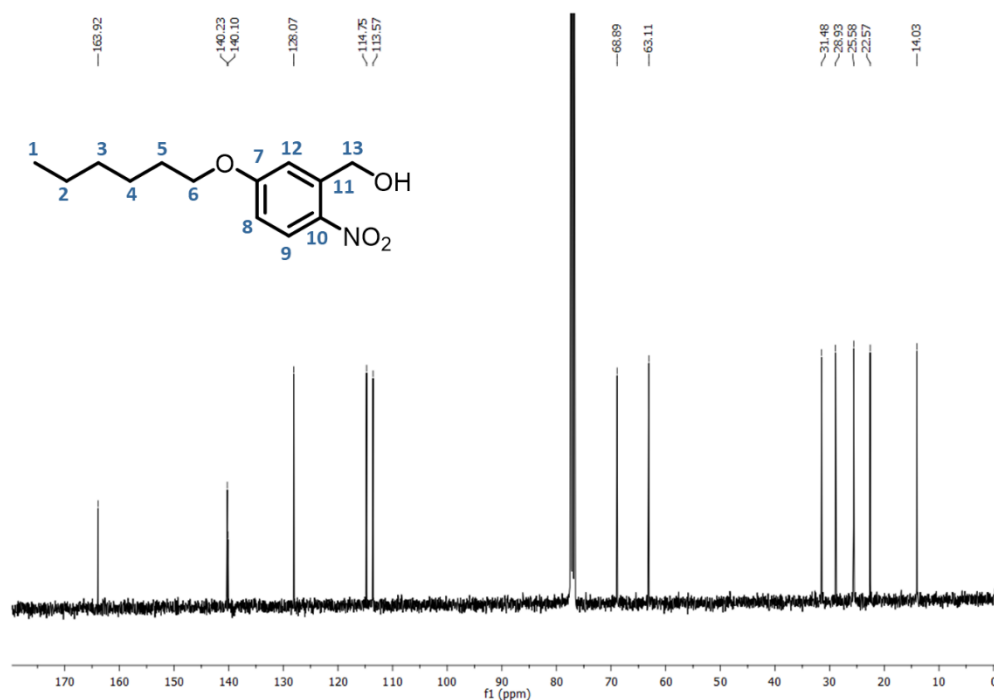
Figure 21. ¹³C NMR spectrum of compound **1** in CDCl₃.
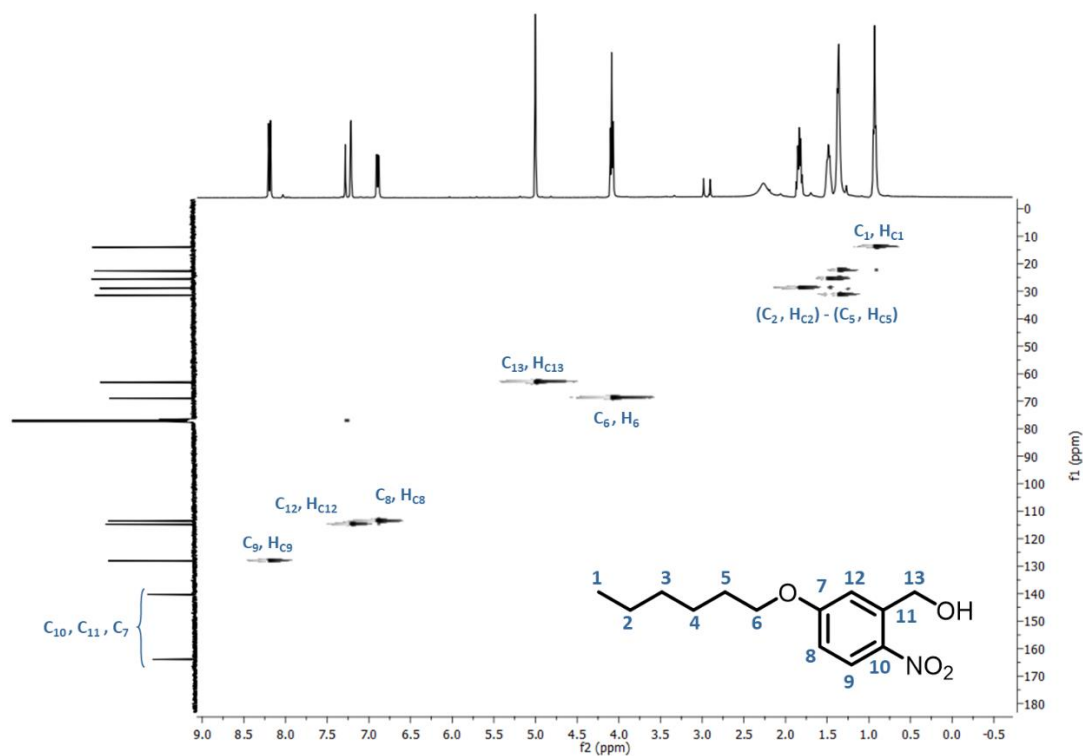
Figure 22. ¹H - ¹³C HSQC spectrum of compound **1** in CDCl₃.

To complete the synthesis of the photocleavable surfactant (compound **2**), compound **1** is dissolved in dry DMF at 0 °C, under argon atmosphere, and NaH is added to remove the proton of the benzylic alcohol and allow the nucleophilic attack to the 3-bromopropyl trimethylammonium.[55] The synthetic procedure is illustrated in **Figure 23**.
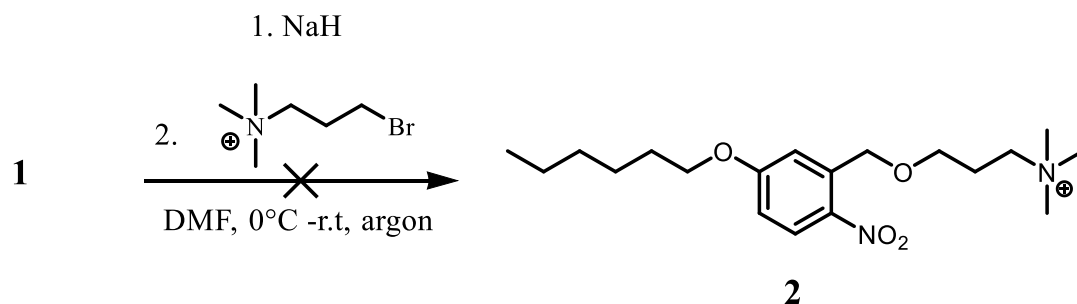
Figure 23. *General procedure for the synthesis of compound 2.*

Several attempts were performed to obtain the required compound. **Table 3** compiles the main results taken from TLC and NMR analysis.

Table 3. *Compilation of the main results obtained from the attempts to prepare compound 2.*

Reactions	Results
Attempt 1	• Product obtained was not compound **2**. • Starting material was degraded to give the aldehyde (F1). • Starting material corresponds to F2 (Figure A.2, Appendix A). • F3 analysis was inconclusive (Figure A.3, Appendix A).
Attempt 2	NMR analysis was inconclusive (Figure A.4, Appendix A).
Attempt 3	Presence of starting material in NMR analysis (Figure A.5, Appendix A).
Attempt 4	NMR analysis was inconclusive (Figure A.6, Appendix A).
Attempt 5	NMR analysis was inconclusive (Figure A.7, Appendix A).
Attempt 6	NMR analysis was inconclusive (Figure A.8, Appendix A).

Attempt 1 was performed based on the protocol described by De Cola et al. [55] Fewer equivalents of base and (3-bromopropyl)trimethylammonium bromide (TAB) were used, since in our case we just desire the reaction of the hydroxy benzyl group, while avoiding the reaction of the phenoxy group. The aromatic ring of the *o*-nitrobenzyl ether group is where the Norrish type II reaction will occur when the compound is subjected to UV-light irradiation, resulting in the specific $O_{bz}-C$ bond cleavage and formation of two products: an alcohol and an aldehyde. Since after three hours of reaction the spot related to the starting material still appeared in the TLC, 1.2 equivalents of base were added, and the reaction was left to stir overnight. To recover the compound after the workup procedure, silica from the preparative plate was scraped off and three stains were recovered (F1, F2 and F3).

The ^1H NMR spectrum of the material extracted from Fraction 1 (F1) of the preparative plate reveals the possible formation of the aldehyde as a product of the photodegradation [62] of the starting material (compound **1**), as demonstrated by the presence of a singlet located at δ 10.51 ppm that corresponds to the proton of an aldehyde and reinforced by the disappearance of the singlet at δ 5.00 ppm related to the two protons connected to C_{13}. Moreover, the peaks corresponding to the three aromatic protons (H_{C9}, H_{C12} and H_{C8}) appear at different chemical shifts when comparing the two spectra (**Figure 24**). The unreacted starting material corresponds to the material extracted from the second stain (Fraction 2 (F2)), as concluded by the analysis of the respective ^1H NMR spectrum (Figure A.2, Appendix A). Another stain was isolated (Fraction 3 (F3)) and studied by NMR analysis, however the ^1H NMR spectrum (Figure A.3, Appendix A) of the extracted material does not allow the identification of any compound.
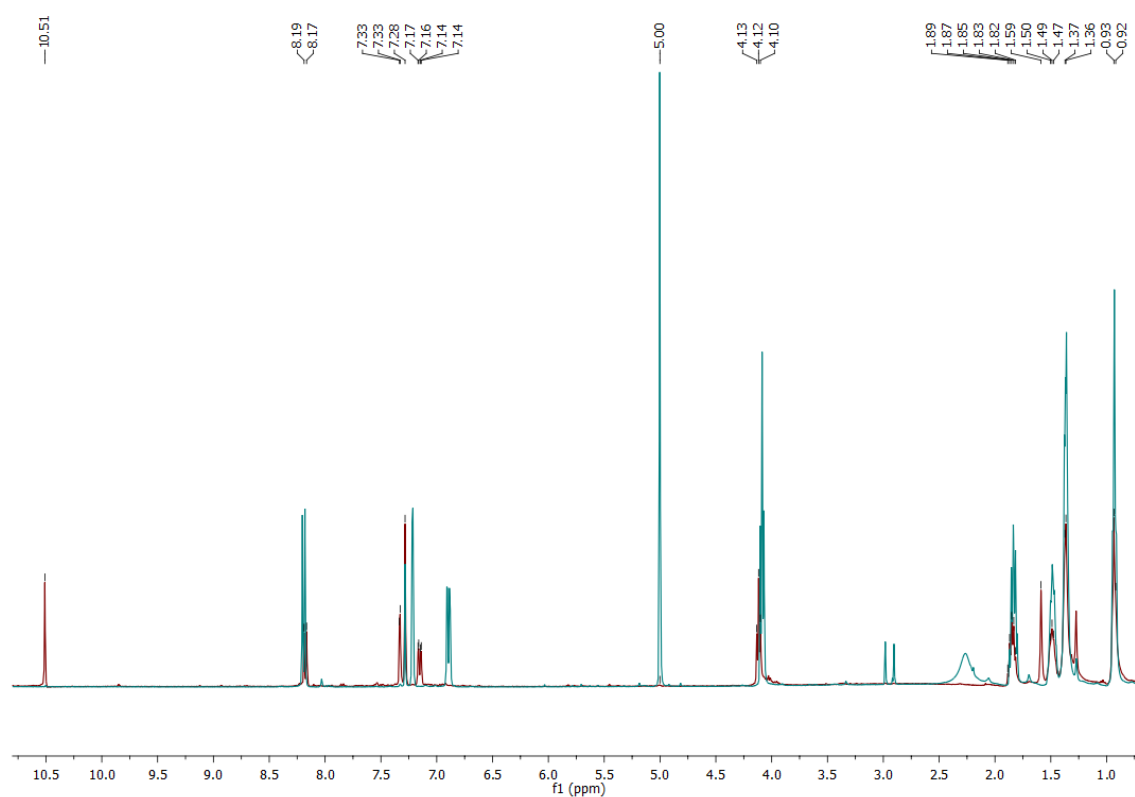

Figure 24. Superposition of ^1H NMR spectra of **1** (blue line) and Fraction 1 (F1) from Attempt 1 (red line) to achieve the light sensitive surfactant (compound **2**), in CDCl₃.

The same procedure as in Attempt 1 was followed for Attempt 2, changing only the ratio between reagents, and after the workup, the reaction crude was analysed by NMR and the ^{1}H NMR spectrum (Figure A.4, Appendix A) did not allow the identification of any compound. In Attempt 3 the same procedure as in Attempt 2 was pursued until 3 h of reaction time, when additional 1.2 equivalents of NaH and 0.5 equivalents of TAB were added to the stirring reaction, and the mixture was left to react overnight at room temperature, under argon atmosphere. The reaction workup was the same as in Attempt 1, and the TLC and NMR results indicate that the reaction did not occur (only starting material was identified). The same peaks characteristic of the starting material can be found in the ^{1}H NMR spectrum of Attempt 3 (Figure A.5, Appendix A), and their integration agrees with the number of protons associated with each peak in the spectrum of the starting material.

In a subsequent effort (Attempt 4), fresh NaH dispersed in mineral oil was used, as the previously used reagent may have degraded due to air exposure. The NMR analysis (Figure A.6 Appendix A), as before, did not allow the identification of any compound. Another attempt was made (Attempt 5), but this time the NaH reagent was pre-washed with hexane to eliminate the mineral oil. The NMR study confirmed that the synthesis was unsuccessful, as no compounds could be identified (Figure A.7, Appendix A). A final experiment was conducted using fresh dry NaH, however it was also not possible to obtain the desired compound and the NMR analysis did not allow the identification of any molecule (Figure A.8, Appendix A).

3.2. Synthesis and characterization of the redox responsive surfactant

The synthesis of the redox responsive surfactant was divided into two steps (**Figure 25**). The first step entails the formation of a disulfide bond between two different thiols, which results in the formation of an unsymmetrical disulfide. To do this, 2-(dimethylamino) ethanethiol and 1-dodecanethiol were reacted to give compound **3** by Base-Catalyzed Aerobic Oxidative Dehydrogenative Coupling. The second step is the methylation of the tertiary amine to give the quaternary ammonium salt (compound **4**).

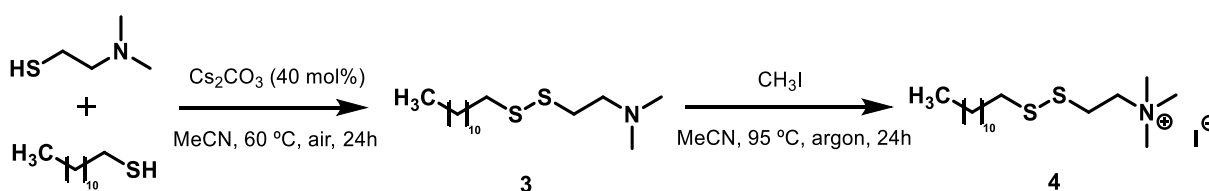***Figure 25.*** *Synthetic scheme for the redox responsive surfactant (compound **4**).*

The difficulty in controlling the chemoselectivity of two different thiols makes the synthesis of unsymmetrical disulfides challenging. The reaction of two different thiols can produce three different products, two resulting from the homocoupling ($\approx$25% yield each based in statistical distribution) and

one resulting from the heterocoupling of the two thiols ($\approx$50% yield based in statistical distribution). Unsymmetrical disulfides can currently be produced using several methods, including the oxidation of thiols, disulfane exchange, nucleophile substitution, oxidative cross-coupling, and opening of thiirane.[63–65] The oxidative cross-dehydrogenative coupling (CDC) reaction is a method that minimizes the number of steps required to produce the desired molecule while allowing the use of straightforward and easily accessible reagents, although the formation of the symmetrical disulfides as by-products resulting from the homocoupling is still inevitable.[64,65]

Lei and colleagues[66] created a method for the oxidant- and catalyst-free electro-oxidative dehydrogenative cross-coupling direct construction of various disulfides. The reaction tolerated a wide range of alkyl mercaptans and produced the desired product in good to high yields but is still very limited to ArS-SAlkyl disulfides. Qiu et al.[64] developed an innovative strategy to synthesise unsymmetrical disulfides through aerobic oxidative CDC of thiols using alkali metal carbonates (M_2CO_3, M = Li, Na, K, Cs) as catalysts. This technique proved to be efficient in synthesizing a wide range of unsymmetrical disulfides, including alkyl disulfides, under mild and ecologically friendly conditions since air is used as an oxidant, and the catalysts used are commercially available and inexpensive.

The synthesis of compound **3** involves the heterocoupling of two different alkyl thiols, which is a difficult reaction to achieve. Qiu et al.[64] managed to obtain unsymmetrical disulfides resulting from the aerobic heterocoupling of functionalized alkyl thiols with tertiary butyl thiol or benzylic thiols catalysed by cesium carbonate, in moderate to high yields. This result encouraged us to devise a synthetic strategy based on their approach to synthesize the desired molecule. The two thiols selected for this work, 2-(dimethylamino) ethanethiol hydrochloride (2-DAT) and 1-dodecanethiol, were combined with cesium carbonate (Cs_2CO_3), in acetonitrile. The mixture was stirred under air, and after the workup, the reaction crude was purified using preparative TLC plates using dichloromethane/ methanol 5% as eluent. The desired product was extracted from the silica with ethyl acetate.

The general protocol was followed with some modifications to achieve the best conditions for the formation of compound **3**, as described in **Table 4**.

Table 4. *Description of different attempts to prepare compound* *3*.

Reaction	Conditions	Observations/ Yield
Attempt 1	Cs_2CO_3 (30 mol%) 2-DAT (1 eq) 1-dodecanethiol (1.1 eq) MeCN, 60°C, air, 42h	η= 31%
Attempt 2	Cs_2CO_3 (20 mol%) 1 eq of 2-DAT 2-DAT (1 eq) 1-dodecanethiol (1.1 eq) MeCN, 80°C, air, 24h	η= 18%

	Cs$_2$CO$_3$ (40 mol%)	
Attempt 3	2-DAT (1 eq)	Best result - reproducible
	1-dodecanethiol (1.1 eq)	**η= 55%**
	MeCN, 60°C, air, 24h	

In Attempt 1, 30 mol% of Cs$_2$CO$_3$, 1 equivalent of 2-DAT and 1.1 equivalents of 1-dodecanethiol were mixed and left to react in acetonitrile for 42h, under air at 60 °C. The reaction was stopped, and after purification, the fraction corresponding to the desired product was analysed by NMR. This procedure proved to be efficient in the preparation of compound **3**, with a yield of 31%. Attempt 2 was performed at a higher temperature using less quantity of catalyst. Since the reaction yield was lower than the obtained in Attempt 1, it was found that in a subsequent reaction it would be preferable to increase the amount of catalyst, keeping the temperature at 60 °C. This was verified in Attempt 3, where 40 mol% of catalyst were used, and after 24h at 60 °C the compound was isolated in 55% yield. This result was the best so far and is comparable to the results reported in the literature for the aerobic heterocoupling of alkyl thiols without a functional group in the α-C. [67] Thus, the procedure described in Attempt 3 was the one chosen to be replicated and used to produce more quantity of compound **3**, highlighting the reproducibility of this method.

The new compound **3** was completely characterized by ^{1}H NMR, ^{13}C NMR, HSQC and ESI[+]-MS analysis.

The ^{1}H NMR spectrum (**Figure 26**) of the resulting product shows three triplets integrating to two protons each, located at δ 2.82 (*J* = 7.9 Hz), δ 2.71 (*J* = 7.1 Hz) and δ 2.63 ppm (*J* = 7.1 Hz) corresponding to carbon atoms number 12, 13, and 14, respectively, as confirmed by the ^{1}H - ^{13}C HSQC spectrum (**Figure 28**). The presence of the six protons corresponding to the two carbon atoms of the tertiary amine (15 and 16) is confirmed by the presence of a singlet at δ 2.29 ppm. The multiplet located at δ 1.72-1.65 ppm is associated to two protons that are connected to C$_{11}$ and the multiplet located at δ 1.41-1.27 ppm corresponds to the 18 protons connected to carbon atoms from the alkyl chain with numbers from 2 to 10. The three protons connected to the last carbon from the alkyl chain (C$_1$) appear as a triplet at δ 0.89 ppm (*J* = 6.7 Hz).
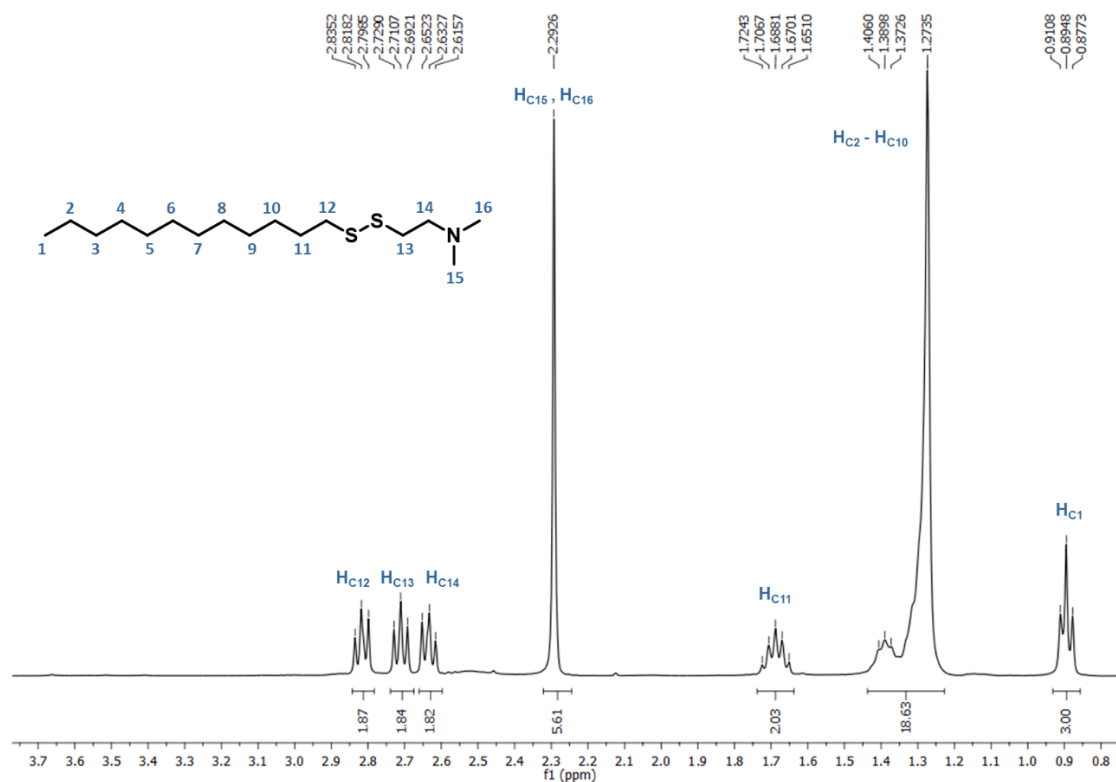
Figure 26. ^1H NMR spectrum of compound **3** in CDCl$_3$.

^{13}C NMR (**Figure 27**) and ^1H - ^{13}C HSQC (**Figure 28**) spectra of compound **3** were analysed, and the peaks at δ 58.8 and 39.2 ppm were assigned to C$_{14}$ and C$_{13}$, respectively. The carbons from the methyl groups connected to the amine (C$_{15}$ and C$_{16}$) both appear at δ 45.3 ppm. The carbon from the hydrophilic part connected to the linker through a C-S bond, appear at δ 36.7 ppm (C$_{12}$). Moreover, the remaining peaks located at δ 29.7 (C$_{11}$), 31.9, 29.7, 29.6, 29.6, 29.5, 29.4, 29.2, 29.2 and 28.6 (C$_{3-10}$), 22.7 (C$_2$) and 14.1 ppm (C$_1$) were assigned to carbons from the alkyl chain.
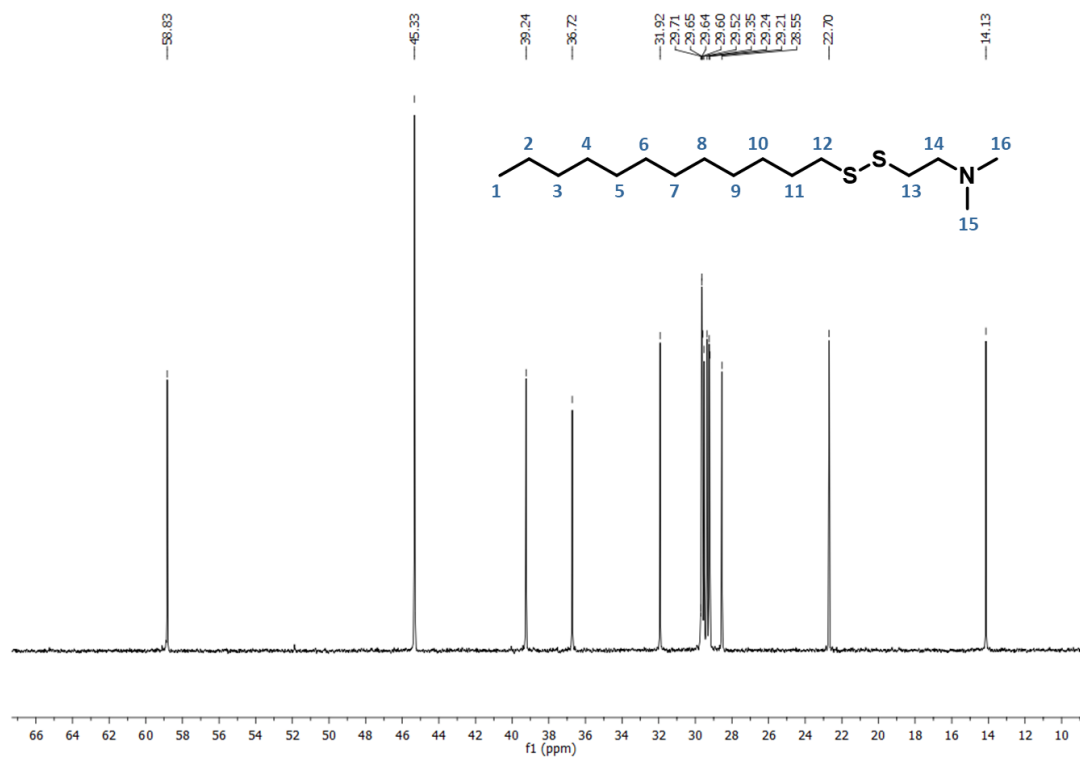
Figure 27. ^{13}C NMR spectrum of compound **3** in CDCl$_3$.
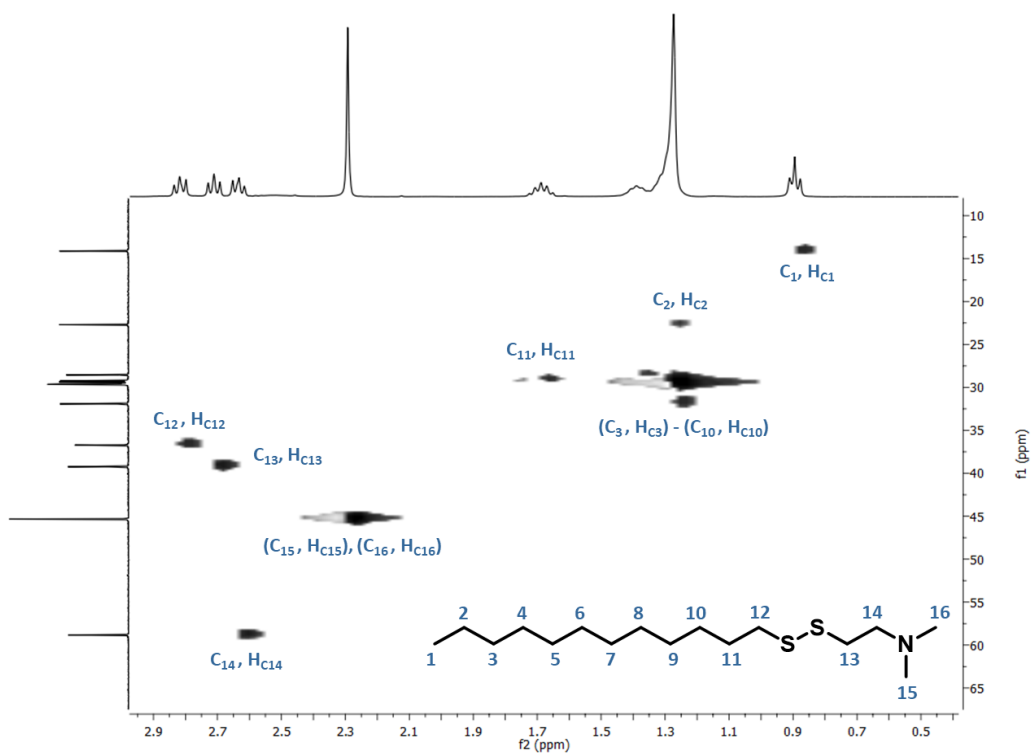
Figure 28. ^1H - ^{13}C HSQC spectrum of compound **3** in CDCl$_3$.

According to ESI+-MS data (Figure A.9, Appendix A), a peak at m/z 306.17, corresponding to the molecular ion [M+H] +, confirms the formation of compound **3**.

The last step to obtain the redox responsive surfactant was the methylation of the tertiary amine to give the quaternary ammonium salt, compound **4**. To accomplish this, compound **3** was combined in acetonitrile with an excess of MeI, under reflux for 24h under argon atmosphere.[67] The excess of MeI and the solvent were evaporated inside the fume hood and the remaining solvent removed in the vacuum line, generating compound **4** in 87 % yield, most likely because of losses during compound recovery.

The analysis of the ^{1}H NMR spectrum of compound **4** (**Figure 29**) reveals that all peaks integrate to the expected values. The protons connected to C_{13} from compound **4** appear on top of the deuterated solvent peak (MeOD), as concluded trough the analysis of the ^{1}H-^{13}C HSQC spectrum of compound **4** (**Figure 32**). A major indicator of the success of the methylation is the presence of a peak at δ 3.26 ppm that integrates to nine protons which agrees with the addition of another methyl group to the tertiary amine, forming the quaternary amine, which has three methyl groups and thus nine protons in the same chemical environment (H_{C15}, H_{C16} and H_{C17}).

The success of the transformation of compound **3** into compound **4** was analysed in more detail by superimposing the ^{1}H NMR spectra of the two compounds (**Figure 30**).
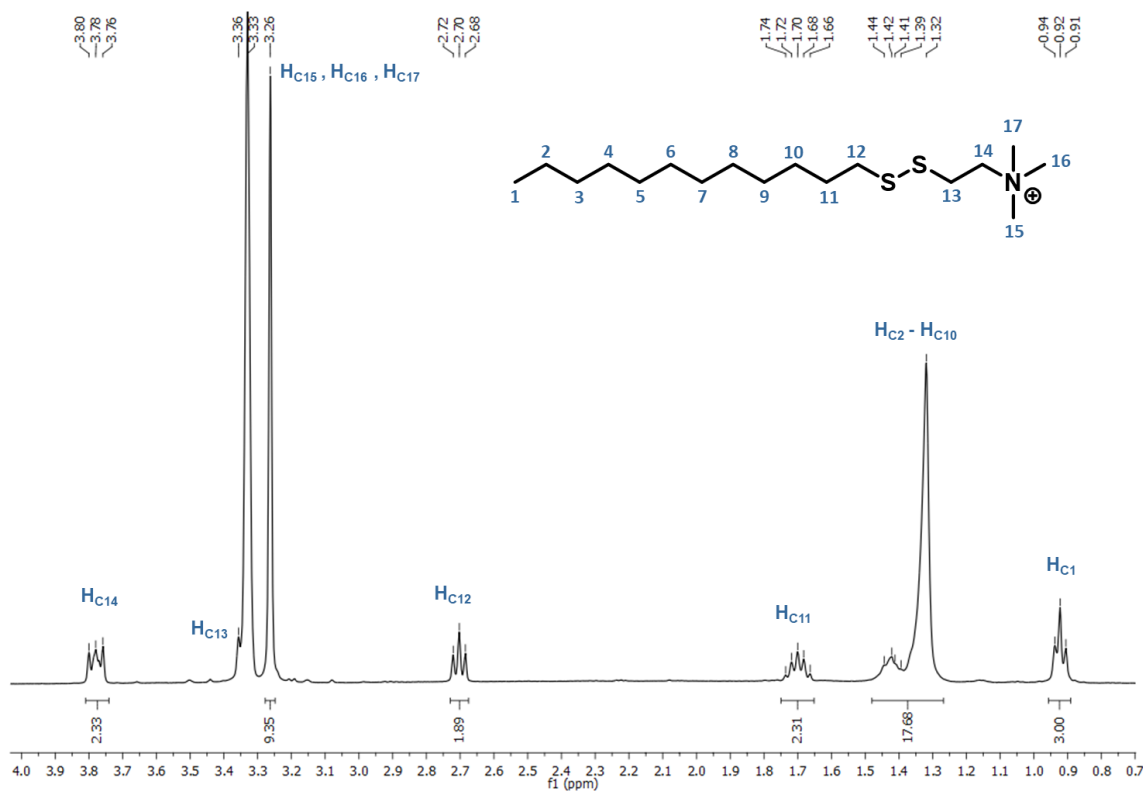
Figure 29. *^{1}H NMR spectrum of compound **4** in MeOD.*

By superimposing the ^1H NMR spectra of compound **3** and **4** is possible to confirm the complete transformation of compound **3** into compound **4**, leading to the formation of a quaternary ammonium ion. The ^1H NMR spectrum of compound **3** in MeOD (Figure A.10, Appendix A) was obtained and analysed to compare both spectra in the same solvent. The protons from the alkyl chain connected to carbons 1-11 on both molecules have practically the same chemical shift while the protons connected to C_{14} (at δ 3.78 ppm (J= 8.76 Hz)) and C_{13} changed to higher chemical shifts after the quaternization of the amine (compound **4**), and the peak that corresponds to the protons from the methyl groups of the amine relocated to a higher field and integrate to nine protons instead of six (compound **3**), highlighting the success of the reaction.
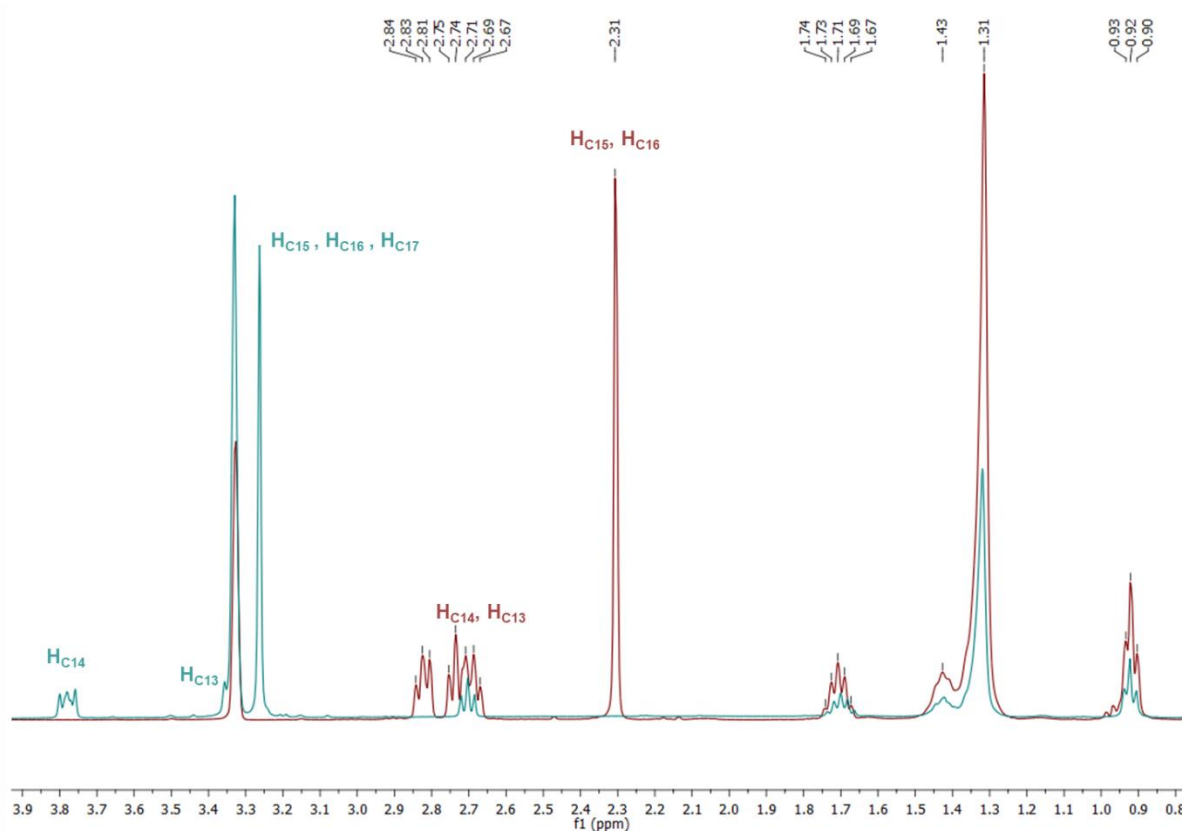
Figure 30. *Superposition of ^1H NMR spectra of compound **3** (red line) and compound **4** (blue line), in MeOD.*

The ^{13}C NMR spectrum of compound **4** (**Figure 31**) does not differ from the ^{13}C NMR spectrum of compound **3** (**Figure 27**), as would be expected since their structures differ only in the presence of an extra methyl group, which is verified by the presence of three peaks in the ^{13}C NMR spectrum of compound **4** at δ 52.7, 52.6 and 52.6 ppm that are related to the three methyl groups (C_{15}, C_{16} and C_{17}) of the quaternary amine (surfactant polar group). The ^1H - ^{13}C HSQC spectrum contributed to the assignment of the remaining carbons. C_{12} and C_{13} appear at δ 38.4 and 30.6 ppm, respectively, in the ^{13}C NMR spectrum of compound **4**. The reaming peaks in the lower field at δ 31.7, 29.4, 29.4, 29.3,

29.2, 29.1, 28.9 and 28.8 (C_{3-10}), 28.0 (C_{11}), 22.3 (C_2) and 13.0 ppm (C_1) correspond to carbons from the hydrophobic part.

Figure 31. ^{13}C NMR spectrum of compound **4** in MeOD.

Figure 32. ^1H- ^{13}C HSQC spectrum of compound **4** in MeOD.

In conclusion, the surfactant was successfully synthesized, as evidenced by the result of the ESI$^+$-MS analysis, showing a peak at m/z 320.14 (Figure A.11, Appendix A) that corresponds to the molecular ion [M]$^+$.

3.2.1. Ionic exchange

After successfully synthesizing compound **4**, an ionic exchange was performed to replace the iodine counterion with chlorine, to improve the compound's water solubility, since our goal is to use this compound as template in the synthesis of MSNs, which is performed in water. After the ionic exchange, a whitish solid (**Figure 33**) was obtained, with a yield of 83% (due to losses during the experimental procedure).

Figure 33. Compound 4 before (left) and after (right) the ionic exchange.

The compound obtained from the ionic exchange, denominated CTAC-SS, was analysed by ^{1}H NMR and ESI$^+$-MS techniques. The ^{1}H NMR spectrum of CTAC-SS (**Figure 34**) has the same profile as the spectrum of compound **4** (**Figure 29**). In the ESI$^+$-MS spectrum of CTAC-SS (**Figure 35**) appears a high intensity peak at m/z 273.05, that could not be attributed to any known fragment, but is also present in the ESI$^+$-MS spectrum of compound **4** (Figure A.11, Appendix A). The peak that corresponds to the molecular ion [M]$^+$ (m/z 320.24) is also present in the ESI$^+$-MS spectrum of CTAC-SS. This data together with the NMR analysis allows us to assume that the compound remains intact during the ionic exchange.
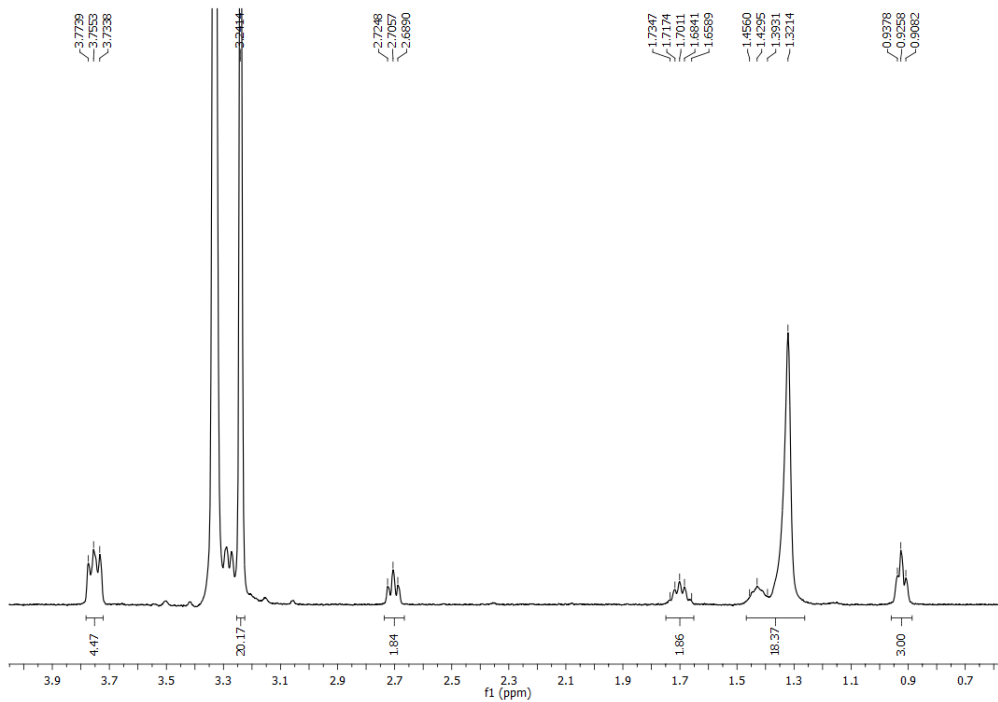
Figure 34. ^{1}H NMR spectrum of CTAC-SS in MeOD.
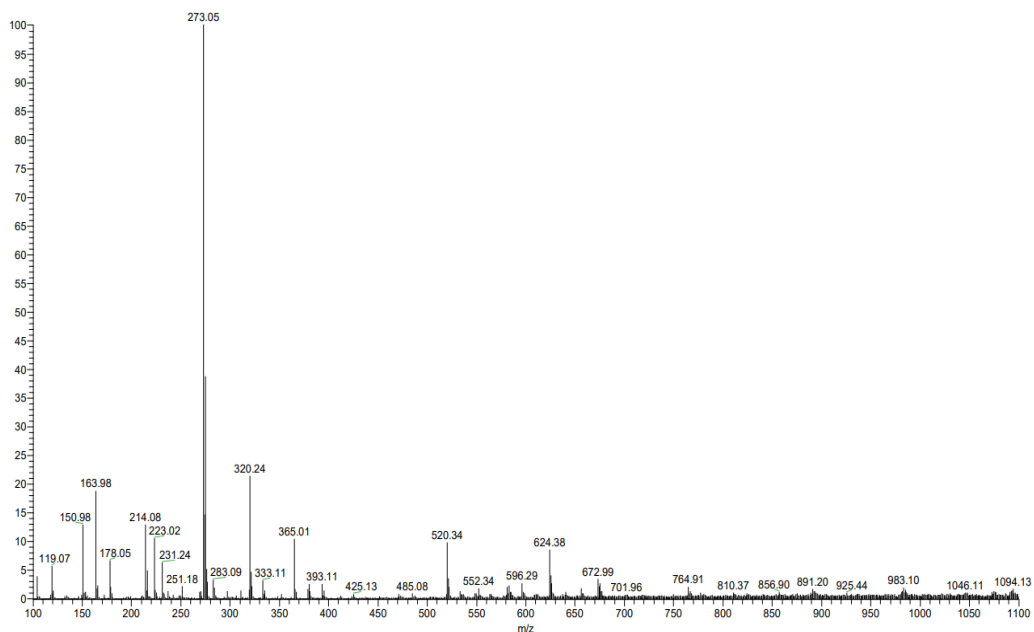
Figure 35. ESI$^+$-MS spectrum of CTAC-SS.

3.2.2. ATR-FTIR and Raman Spectroscopy

CTAC-SS was analysed by ATR-FTIR and Raman spectroscopy to confirm the presence of the disulfide bond (-S-S-) in the compound's structure. In the infrared spectra of 2-(dimethylamino) ethanethiol hydrochloride (2-DAT) (**Figure 36A**) it is possible to see the characteristic peak of the thiol group (-SH) at 2560 cm^{-1},[68] that is not present in the spectrum of CTAC-SS (**Figure 36B**).
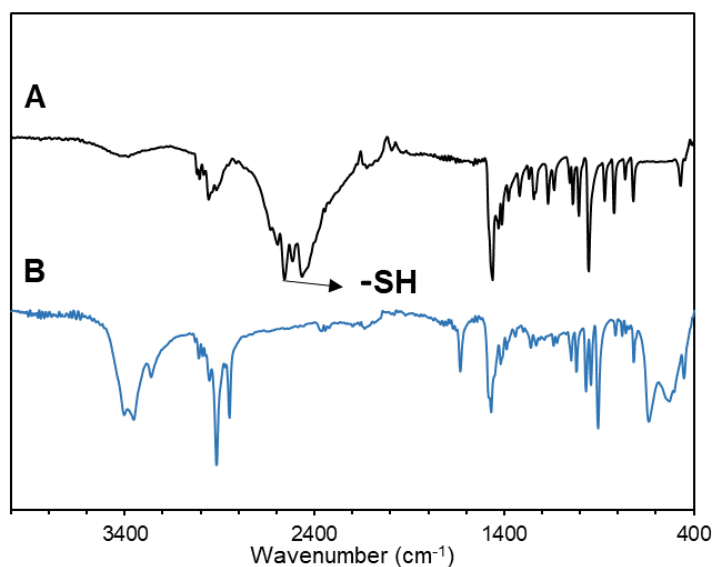
Figure 36. ATR-FTIR spectra of 2-DAT (*A*) and CTAC-SS (*B*).

In the Raman spectrum of CTAC-SS appears a clear Raman signal at 511 cm^{-1} (**Figure 37A**) which is related to the presence of a disulfide bond in the molecule. As expected, a signal at 2577 cm^{-1} (-SH) is present in the spectrum of 1-dodecanethiol (**Figure 37C**), and no signal related to the thiol group appears in the spectrum of CTAC-SS (**Figure 37B**).[69]

These results confirm the presence of a disulfide bond in CTAC-SS and eliminate the possibility of contamination with the starting materials, thus reinforcing the success of the synthesis of compound **4**, and confirming the success of the ionic exchange, which culminates in the formation of CTAC-SS.

CTAC-SS
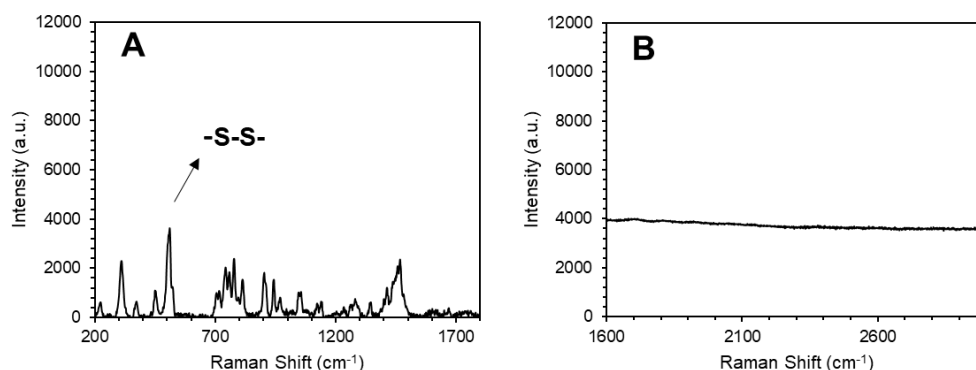
1-dodecanethiol
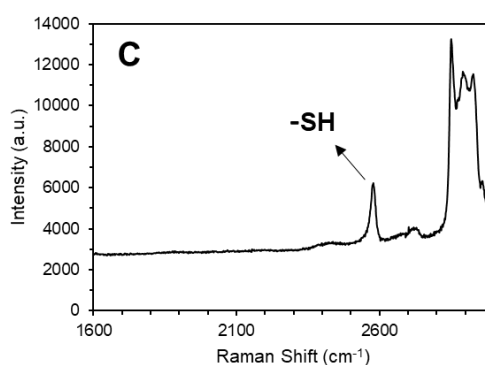
*Figure 37. Raman spectra of CTAC-SS - 532 nm excitation (**A**) and 633 nm excitation (**B**)- and 1-dodecanethiol (**C**).*

3.3. Preliminary studies with CTAC-SS

After successfully synthesizing the redox responsive surfactant, some preliminary studies were carried out to estimate the behaviour of CTAC-SS as a smart surfactant in solution: its ability to form micelles and the type of micelles that are formed, its critical micelle concentration (CMC), and its response to the respective stimulus, i.e., the degradation of the compound in the presence of a reducing agent.

3.3.1. Degradation studies for CTAC-SS

Once the stimuli responsive surfactant (CTAC-SS) is synthesized and characterized, it is necessary to verify its cleavage when subjected to the respective stimulus. As verified above, CTAC-SS contains a disulfide bond that acts as the target group, being responsible for the degradation of the surfactant. Dithiothreitol is a strong but mild reducing agent, with a low redox potential of -0.332 V at pH 7, that undergoes oxidation in the presence of disulfide bonds, resulting in the formation of a cyclic molecule

(*ox*-DTT), a stable six-membered ring with an internal disulfide bond, which exhibits a characteristic absorption band at 283 nm.[70,71] CTAC-SS in the presence of *red*-DTT suffers cleavage of the S-S bond, which results in the formation of two thiols, and simultaneously *red*-DDT is oxidized to *ox*-DTT, as depicted in **Figure 38**.

Figure 38. *Schematic representation of the degradation of CTAC-SS in the presence of DTT.*

Aqueous solutions of CTAC-SS and DTT were prepared at pH 7, since DTT has an optimal pH range between 7.1 and 8.0, although the reagent can be effectively used at pH 6.5-9.0. [72,73] The absorption of the mixture (1.25 mM of CATAC-SS + 5 mM of DTT) was recorded at a fixed wavelength (λ= 283 nm), where the characteristic absorption band of *ox*-DTT appears, each 2 s for 30 minutes and the results are compiled in **Figure 39A**. Absorbance increases until it reaches a constant value, that corresponds to the complete cleavage of all disulfide bonds present in solution, confirming that DTT can be used to degrade our surfactant. After 30 min an absorption spectrum of the mixture was recorded, where is possible to visualize the characteristic absorption band of *ox*-DTT (**Figure 39B**). The absorption spectrum of the CTAC-SS aqueous solution (1.25 mM) at pH 7 is also shown in **Figure 39B**, to prove that the isolated compound is not responsible for the band at 283 nm, which appears only in the presence of DTT.

Figure 39. *Absorbance at λ= 283 nm over 30 minutes of an aqueous solution of CTAC-SS (1.25 mM) and DTT (5 mM), at pH 7 (**A**); Absorption spectrum of an aqueous solution of CTAC-SS (1.25 mM) and DTT (5 mM) at pH 7, after 30 minutes, and an aqueous solution of CTAC-SS (1.25 mM) at pH 7(**B**).*

The absorption spectra of aqueous solutions of DTT (5mM) and CTAC-SS (1.25 mM) at pH 7 were measured separately each 5 minutes for 30 minutes and the results (Appendix B, Figure B.1.) confirm that the band present at 283 nm is only due to the oxidation of DTT in the presence of S-S bonds, since no band appears at this wavelength and no change is evident in the spectra of the isolated solutions during the same period as the spectrum of the mixture was recorded.

3.3.2. Computational studies

Geometry optimization of CTAB and CTAC-SS was performed, and the respective optimized structures are presented in **Figure 40**. The structure of CTAC-SS differs from the structure of CTAB, due to the presence of the disulfide bond that causes the molecule to bend.
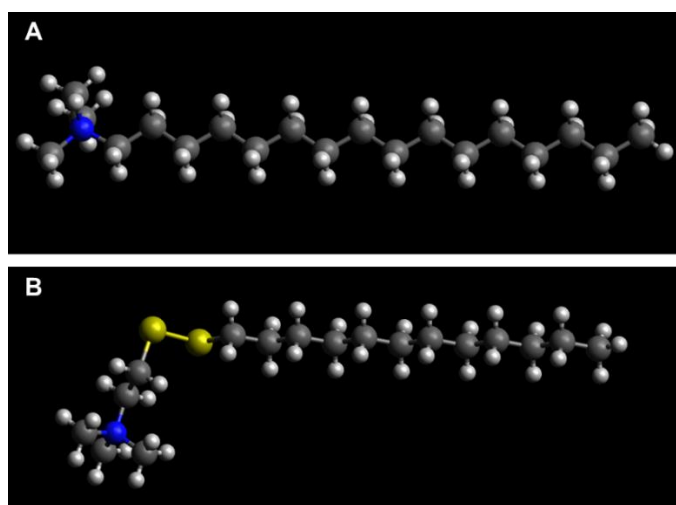

Figure 40. *Optimized structure of CTAB (A) and CTAC-SS (B). Yellow, blue, grey, and white atoms represent sulphur, nitrogen, carbon, and hydrogen atoms, respectively.*

From the optimized structures it was possible to make an approximate calculation of the critical packing parameter (cpp) (Equation 4) of both surfactants (**Figure 41**). The volume of the hydrophobic part was calculated considering the volume of a truncated cone, with a larger base that corresponds to the hydrophobic/hydrophilic interface. In the case of CTAB, the height (h) of the cone corresponds to the distance between the last hydrogen atom of the hydrophobic chain and the nitrogen atom of the hydrophobic group, while for CTAC-SS the heigth (h) of the cone was defined as the distance between the last hydrogen atom of the hydrophobic chain and the sulphur atom close to the hydrophilic group. The value obtained for CTAB was 0.53, which is higher than expected since CTAB forms cylindrical micelles (0.33<cpp<0.5), and for CTAC-SS was 0.46, indicating that this surfactant will form cylindrical micelles.
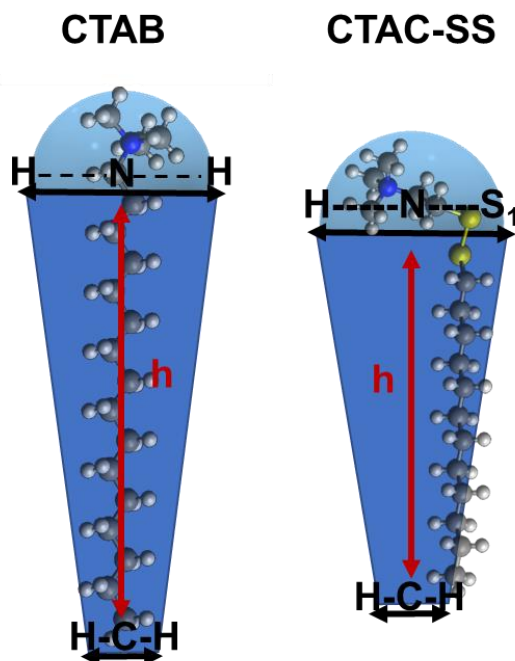
Figure 41. *Schematic representation of the method used to calculate the critical packing parameter (cpp) of CTAB (left) and CTAC-SS (right).*

3.3.3. Determination of the critical micelle concentration (CMC) of CTAC-SS

Measurements of the surface tension of a set of solutions with different concentrations (3.5 - 0.05 mM) were made to find the dependence of the surface tension on concentration, to calculate the CMC value. The range of concentration values was defined based on the CMC of CTAB (1 mM) [74], due to the structure similarity between the two surfactants. **Table 5** compile the mean surface tension values obtained using the pendant drop method for the specified concentration range, as well as the standard deviation for the 140 measurements taken for each solution.

Table 5. *Values of mean surface tension for the solutions with different concentration of CTAC-SS.*

	[CTAC-SS] (mM)	γ (mN/m)	log ([CTAC-SS] /mM))
	0.05	68.57 ± 0.28	-1.3
	0.1	68.29 ± 0.22	-1
	0.2	68.56 ± 0.21	-0.70
CTAC-SS	0.4	68.36 ± 0.23	-0.40
(pH 7)	0.6	68.21 ± 0.19	-0.22
	0.8	68.25 ± 0.30	-0.10
	1.5	67.64 ± 0.24	0.18
	3.5	62.13 ± 0.54	0.54

The mean surface tension values were plotted as a function of the logarithm of the concentration of CTAC-SS (**Figure 42**). A decrease in surface tension was expected with log ([CTAC-SS]) until the value corresponding to the CMC was reached, with constant surface tension above the CMC. However, the CTAC-SS results were not as expected. Surface tension remained constant as concentration increased up to 3.5 mM. These results allow us to speculate on possible behaviors of CTAC-SS in solution.

Since the surface tension value for CTAC is very similar to the value of reference for water (72.75 mN/m) [57], we can infer that CTAC-SS molecules do not adsorb at the surface. One hypothesis is the existence of a very high CMC, therefore the chosen concentration range would be far below the CMC, where little adsorption at the surface would be observed. On the other hand, the practically unchanged surface tension could be explained by a very low CMC, with the formation of micelles at very low concentrations, but without surfactant adsorption to the air-water interface. The performance of CTAC-SS in solution is therefore ambiguous, requiring more data to assess its behavior as a surfactant and to calculate its CMC.
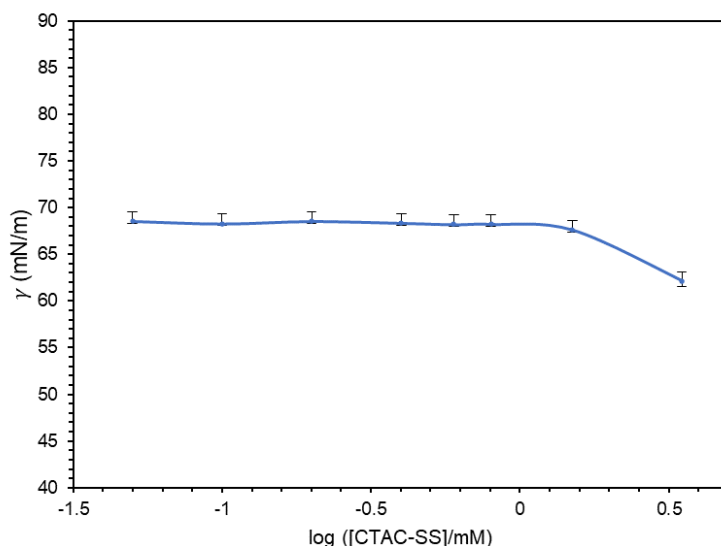

Figure 42. *Surface tension of CTAC-SS as a function of the logarithm of the concentration.*

3.3.4. Dynamic Light Scattering

Dynamic Light Scattering of CTAC-SS solutions was performed to check if there was any self-assembling of the CTAC-SS, and to obtain the hydrodynamic diameter of the formed structures. The correlograms and the results of the size distribution by number are shown in **Figure 43** and **Figure 44**, respectively.

Trought the analysis of the correlogram of CTAC-SS dispersions with concentrations 1.67 mM, 1 mM, 0.8 mM, and 0.6 mM, it is possible to conclude that all dispersions are polydisperse, since the decay of the correlation curve is extended in all cases, which indicates larger polydispersity of the

samples. Moreover, the size distribution by number of each solution has only one peak, meaning that in solution there is only a population of particles with similar diameters. The mean hydrodynamic diameter of the particles present in CTAC-SS dispersions is 47 ± 5 nm, which indicates that the particles present in the solutions with different concentrations have consistent sizes, and although the surface tension results indicate that there is no adsorption at the surface, there seems to exist formation of micelles in solution.
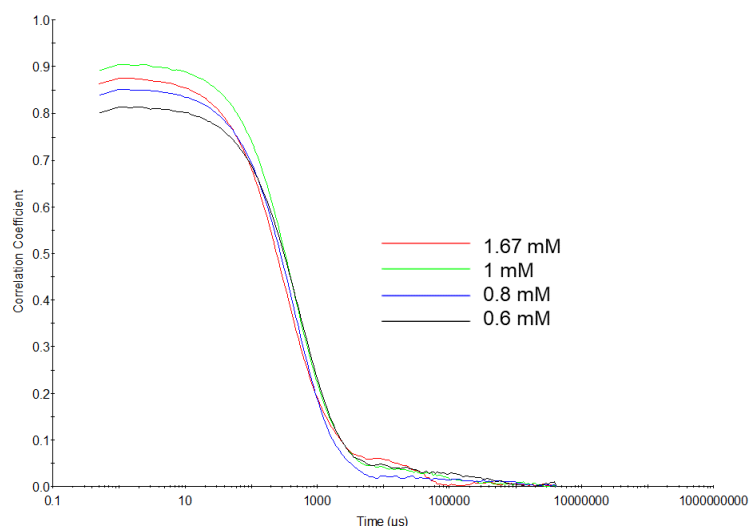

Figure 43. Correlogram of CTAC-SS solutions: 1.67 mM, 1 mM, 0.8 mM, and 0.6 mM.
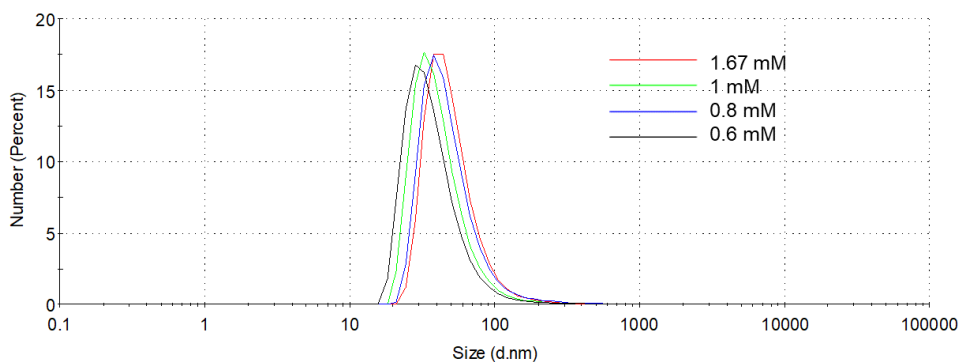

Figure 44. Size distribution by number of CTAC-SS solutions: 1.67 mM, 1 mM, 0.8 mM, and 0.6 mM.

The results of the geometry optimization (**Section 3.3.2**) indicate a cpp consistent with the formation of cylindrical micelles, which means that the particles present in solution are not spherical. The hydrophobic part of CTAC-SS has approximately 2 nm of length and particles found in the DLS analysis have a hydrodynamic radius of 23.5 nm which is another indicator that the micelles formed couldn't be spherical. In that case the hydrodynamic diameter obtained in the DLS analysis corresponds to the diameter of a sphere that has the same translational diffusion coefficient as the CTAC-SS micelles. Considering the formation of cylindrical micelles, the radius of the micelle (R) can be defined as the length of the hydrophobic part (2 nm) and the length (L) of the micelle can be determined through the

relationship between the hydrodynamic radius (R_H) and the radius of gyration (R_g). (Equations 5 and 6).[75,76]

$$\frac{R_g}{R_H} = \frac{1}{\sqrt{3}} \ln\left(\frac{L}{2R} - 0.5\right) \qquad (5)$$

$$R_g{}^2 = \frac{R^2}{2} + \frac{L^2}{12} \qquad (6)$$

The value obtained for the length of the micelle was 261 nm, considering a rigid structure (fully stretched). The micelle length is then lower than 261 nm since the micelle can be in a wormlike conformation (not a rigid cylinder).
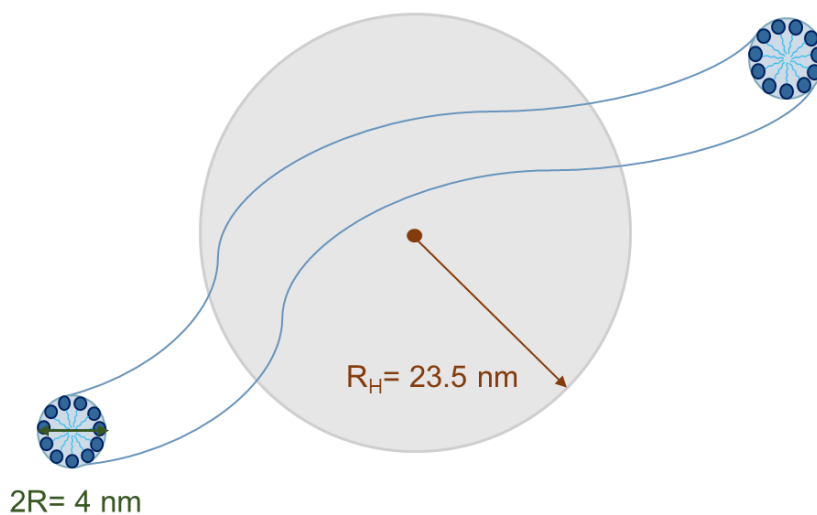

Figure 45. Schematic representation of a wormlike micelle with L<261 nm.

Conclusions

The goal of this work was to design a novel smart surfactant with hydrophilic and hydrophobic moieties that are cleavable in response to a stimulus. This surfactant would satisfy the necessary conditions to integrate the two-surfactant system used in the strategy for the synthesis of dual pore MSNs. A light responsive surfactant and a redox responsive surfactant were chosen, and simple synthetic schemes were devised to obtain both molecules in just two steps.

The synthesis of the light responsive surfactant was not successful, because of the instability of the substrate during the second step of the synthesis. In the case of the redox responsive surfactant, the product was successfully synthesized in two steps. The intermediate and the final molecule were obtained in moderate to high yields and characterized by ^{1}H NMR, ^{13}C NMR, HSQC spectroscopy and by ESI$^+$-MS.

After successfully synthesizing the iodine salt of the redox-responsive surfactant, an ionic exchange was undertaken to replace the iodine counterion with chlorine to increase the compound's solubility in water, originating a whitish solid in high yield, denominated CTAC-SS. This compound was characterized by ^{1}H NMR, ESI$^+$-MS, ATR-FTIR and Raman, proving its integrity during the ionic exchange.

Some preliminary studies with CTAC-SS were conducted to evaluate its behavior as a smart surfactant. Geometry optimization of CTAB and CTAC-SS were performed, and the critical packing parameter (cpp) values of both surfactants were estimated. The cpp obtained for CTAB was 0.53 and for CTAC-SS was 0.46, which indicate that using the same approximations for the calculation of the cpp for both molecules, the results are similar despite the differences in their structure. Most probably, CTAC-SS will form cylindrical micelles. Degradability tests were conducted, and the results show that CTAC-SS disulfide bond suffers cleavage in the presence of dithiothreitol (DTT). After 30 minutes in the presence of the reducing agent, it was possible to observe the characteristic absorption band of *ox*-DTT at 283 nm, which is an indicator of the degradability of CTAC-SS.

The surface tension of solutions of CTAC-SS was measured using the pendant drop method. The surface tension did not change within the range of 0.05 mM - 3.5 mM CTAC-SS concentrations. These results were not conclusive on the behavior of CTAC-SS in solution, and it was not possible to calculate de CMC of CTAC-SS from the plot of surface tension as a function of the logarithm of the concentration. Possible explanations are that either the molecule does not absorb to the liquid-gas interface but forms micelles; or the CMC is very high (out of the range tested). However, DLS results of CTAC-SS solutions reveal the presence of particles with 47 ± 5 nm of mean hydrodynamic diameter, which, if cylindrical micelles are formed as predicted by the cpp, correspond to the formation of cylindrical micelles with a maximum length of 261 nm.

The overall results highlight the success of this work and indicate that CTAC-SS can be a promising smart surfactant with broad applications, such as in the synthesis of dual pore MSNs and other nanostructures. Nonetheless, the preliminary results still leave some questions to be clarified about the

behavior of CTAC-SS as a surfactant, which can be addressed by conducting additional research and refining previous studies.

In future work, it would be interesting to verify the formation of MSNs using this surfactant as template, and later combine it with an inert surfactant to produce the desired dual pore MSNs. The strategy is to use CTAC-SS, an alkyl cleavable surfactant, together with a perfluorinated "inert" surfactant, such as HFDePC[14], taking advantage of the poor miscibility of the fluorocarbon and hydrocarbon chains, thus avoiding the formation of mixed micelles.[14]

References

(1)   Gonçalves, M. Sol-Gel Silica Nanoparticles in Medicine: A Natural Choice. Design, Synthesis and Products. *Molecules* **2018**, *23* (8), 2021. https://doi.org/https://doi.org/10.3390/molecules23082021.

(2)   Jeelani, P. G.; Mulay, P.; Venkat, R.; Ramalingam, C. Multifaceted Application of Silica Nanoparticles. A Review. *Silicon* **2020**, *12* (6), 1337–1354. https://doi.org/https://doi.org/10.1007/s12633-019-00229-y.

(3)   Rahman, I. A.; Padavettan, V. Synthesis of Silica Nanoparticles by Sol-Gel: Size-Dependent Properties, Surface Modification, and Applications in Silica-Polymer Nanocomposites—A Review. *J. Nanomater.* **2012**, *2012*, 132424. https://doi.org/10.1155/2012/132424.

(4)   Bitar, A.; Ahmad, N. M.; Fessi, H.; Elaissari, A. Silica-Based Nanoparticles for Biomedical Applications. *Drug Discov. Today* **2012**, *17* (19–20), 1147–1154. https://doi.org/https://doi.org/10.1016/j.drudis.2012.06.014.

(5)   Liberman, A.; Mendez, N.; Trogler, W. C.; Kummel, A. C. Synthesis and Surface Functionalization of Silica Nanoparticles for Nanomedicine. *Surf. Sci. Rep.* **2014**, *69* (2–3), 132–158. https://doi.org/https://doi.org/10.1016/j.surfrep.2014.07.001.

(6)   Mohajerani, A.; Burnett, L.; Smith, J. V; Kurmus, H.; Milas, J.; Arulrajah, A.; Horpibulsuk, S.; Abdul Kadir, A. Nanoparticles in Construction Materials and Other Applications, and Implications of Nanoparticle Use. *Materials (Basel).* **2019**, *12* (19), 3052. https://doi.org/https://doi.org/10.3390/ma12193052.

(7)   Baig, N.; Kammakakam, I.; Falath, W. Nanomaterials: A Review of Synthesis Methods, Properties, Recent Progress, and Challenges. *Mater. Adv.* **2021**, *2* (6), 1821–1871. https://doi.org/https://doi.org/10.1039/D0MA00807A.

(8)   Catauro, M.; Ciprioti, S. V. Characterization of Hybrid Materials Prepared by Sol-Gel Method for Biomedical Implementations. A Critical Review. *Materials (Basel).* **2021**, *14* (7), 1788. https://doi.org/https://doi.org/10.3390/ma14071788.

(9)   Kumar, A.; Yadav, N.; Bhatt, M.; Mishra, N. K.; Chaudhary, P.; Singh, R. Sol-Gel Derived Nanomaterials and It's Applications: A Review. *Res. J. Chem. Sci.* **2015**, *2231*, 606X.

(10)   Loryuenyong, V.; Muanghom, T.; Apinyanukul, T.; Rutthongjan, P. Synthesis of Templated Mesoporous Silica Nanoparticles under Base Catalysis. *Adv. Appl. Ceram.* **2011**, *110* (6), 335–339. https://doi.org/https://doi.org/10.1179/1743676111Y.0000000024.

(11)   Bokov, D.; Turki Jalil, A.; Chupradit, S.; Suksatan, W.; Javed Ansari, M.; Shewael, I. H.; Valiev, G. H.; Kianfar, E. Nanomaterial by Sol-Gel Method: Synthesis and Application. *Adv. Mater. Sci. Eng.* **2021**, *2021*. https://doi.org/https://doi.org/10.1155/2021/5102014.

(12)   Narayan, R.; Nayak, U. Y.; Raichur, A. M.; Garg, S. Mesoporous Silica Nanoparticles: A Comprehensive Review on Synthesis and Recent Advances. *Pharmaceutics* **2018**, *10* (3), 1–49. https://doi.org/10.3390/pharmaceutics10030118.

(13)   Gonçalves, J. L. M.; Baleizão, C.; Farinha, J. P. S. Smart Porous Silica–Polymer Nanomaterials for Theranostics. *Soft Matter Biomed. Appl.* **2021**, *13*, 365.

(14)   Canadas, C. Hybrid Nanocontainer with Dual Control Release System, Masther's Thesis, Universidade de Lisboa, 2021.

(15)   Ghimire, P. P.; Jaroniec, M. Renaissance of Stöber Method for Synthesis of Colloidal Particles: New Developments and Opportunities. *J. Colloid Interface Sci.* **2021**, *584*, 838–865. https://doi.org/https://doi.org/10.1016/j.jcis.2020.10.014.

(16)   Valtchev, V.; Tosheva, L. Porous Nanosized Particles: Preparation, Properties, and Applications. *Chem. Rev.* **2013**, *113* (8), 6734–6760. https://doi.org/10.1021/cr300439k.

(17)   Wu, S. H.; Lin, H. P. Synthesis of Mesoporous Silica Nanoparticles. *Chem. Soc. Rev.* **2013**, *42* (9), 3862–3875. https://doi.org/10.1039/c3cs35405a.

(18)   Chiang, Y.-D.; Lian, H.-Y.; Leo, S.-Y.; Wang, S.-G.; Yamauchi, Y.; Wu, K. C.-W. Controlling Particle Size and Structural Properties of Mesoporous Silica Nanoparticles Using the Taguchi Method. *J. Phys. Chem. C* **2011**, *115* (27), 13158–13165. https://doi.org/https://doi.org/10.1021/jp201017e.

(19)   Kajihara, K. Recent Advances in Sol–Gel Synthesis of Monolithic Silica and Silica-Based Glasses. *J. Asian Ceram. Soc.* **2013**, *1* (2), 121–133. https://doi.org/https://doi.org/10.1016/j.jascer.2013.04.002.

(20)   Yamamoto, E.; Kuroda, K. Colloidal Mesoporous Silica Nanoparticles. *Bull. Chem. Soc. Jpn.* **2016**, *89* (5), 501–539. https://doi.org/10.1246/bcsj.20150420.

(21)   Mehmood, A.; Ghafar, H.; Yaqoob, S.; Gohar, U. F.; Ahmad, B. Mesoporous Silica Nanoparticles: A Review. *J. Dev. Drugs* **2017**, *6* (02). https://doi.org/10.4172/2329-6631.1000174.

(22)   Bari, A. H.; Jundale, R. B.; Kulkarni, A. A. Understanding the Role of Solvent Properties on Reaction Kinetics for Synthesis of Silica Nanoparticles. *Chem. Eng. J.* **2020**, *398*, 125427. https://doi.org/https://doi.org/10.1016/j.cej.2020.125427.

(23)   Rastegari, E.; Hsiao, Y. J.; Lai, W. Y.; Lai, Y. H.; Yang, T. C.; Chen, S. J.; Huang, P. I.; Chiou, S. H.; Mou, C. Y.; Chien, Y. An Update on Mesoporous Silica Nanoparticle Applications in Nanomedicine. *Pharmaceutics* **2021**, *13* (7), 1–56. https://doi.org/10.3390/pharmaceutics13071067.

(24)   Pal, N.; Lee, J.-H.; Cho, E.-B. Recent Trends in Morphology-Controlled Synthesis and Application of Mesoporous Silica Nanoparticles. *Nanomaterials* **2020**, *10* (11), 2122. https://doi.org/10.3390/nano10112122.

(25)   Ribeiro, T.; Rodrigues, A. S.; Calderon, S.; Fidalgo, A.; Gonçalves, J. L. M.; André, V.; Teresa Duarte, M.; Ferreira, P. J.; Farinha, J. P. S.; Baleizão, C. Silica Nanocarriers with User-Defined Precise Diameters by Controlled Template Self-Assembly. *J. Colloid Interface Sci.* **2020**, *561*, 609–619. https://doi.org/10.1016/j.jcis.2019.11.036.

(26)   Mekaru, H.; Lu, J.; Tamanoi, F. Development of Mesoporous Silica-Based Nanoparticles with Controlled Release Capability for Cancer Therapy. *Adv. Drug Deliv. Rev.* **2015**, *95*, 40–49. https://doi.org/10.1016/j.addr.2015.09.009.

(27)   Savic, S.; Vojisavljević, K.; Počuča-Nešić, M.; Živojević, K.; Mladenovic, M.; Knezevic, N. Hard Template Synthesis of Nanomaterials Based on Mesoporous Silica. *Metall. Mater. Eng.* **2018**, *24*. https://doi.org/10.30544/400.

(28)   Dutt, S.; Siril, P. F.; Remita, S. Swollen Liquid Crystals (SLCs): A Versatile Template for the Synthesis of Nano Structured Materials. *RSC Adv.* **2017**, *7* (10), 5733–5750. https://doi.org/10.1039/C6RA26390A.

(29)   Andreani, T.; Silva, A. M.; Souto, E. B. Silica-based Matrices: State of the Art and New Perspectives for Therapeutic Drug Delivery. *Biotechnol. Appl. Biochem.* **2015**, *62* (6), 754–764. https://doi.org/10.1002/bab.1322.

(30)   Barczak, M. Template Removal from Mesoporous Silicas Using Different Methods as a Tool for Adjusting Their Properties. *New J. Chem.* **2018**, *42* (6), 4182–4191. https://doi.org/10.1039/c7nj04642a.

(31)   Yu, H.; Zhang, Q.; Dahl, M.; Joo, J. B.; Wang, X.; Wang, L.; Yin, Y. Dual-Pore Carbon Shells for Efficient Removal of Humic Acid from Water. *Chem. - A Eur. J.* **2017**, *23* (64), 16249–16256. https://doi.org/10.1002/chem.201702318.

(32)   Hwang, L.; Guardado-Alvarez, T. M.; Ayaz-Gunner, S.; Ge, Y.; Jin, S. A Family of Photolabile Nitroveratryl-Based Surfactants That Self-Assemble into Photodegradable Supramolecular Structures. *Langmuir* **2016**, *32* (16), 3963–3969. https://doi.org/10.1021/acs.langmuir.6b00658.

(33) Carvalho, G. C.; Sábio, R. M.; de Cássia Ribeiro, T.; Monteiro, A. S.; Pereira, D. V.; Ribeiro, S. J. L.; Chorilli, M. Highlights in Mesoporous Silica Nanoparticles as a Multifunctional Controlled Drug Delivery Nanoplatform for Infectious Diseases Treatment. *Pharm. Res.* **2020**, *37* (10), 191. https://doi.org/10.1007/s11095-020-02917-6.

(34) Niu, D.; Ma, Z.; Li, Y.; Shi, J. Synthesis of Core-Shell Structured Dual-Mesoporous Silica Spheres with Tunable Pore Size and Controllable Shell Thickness. *J. Am. Chem. Soc.* **2010**, *132* (43), 15144–15147. https://doi.org/10.1021/ja1070653.

(35) Groenewolt, M.; Antonietti, M.; Polarz, S. Mixed Micellar Phases of Nonmiscible Surfactants: Mesoporous Silica with Bimodal Pore Size Distribution via the Nanocasting Process. *Langmuir* **2004**, *20* (18), 7811–7819. https://doi.org/10.1021/la049147k.

(36) Sun, J.; Shan, Z.; Maschmeyer, T.; Moulijn, J. A.; Coppens, M. O. Synthesis of Tailored Bimodal Mesoporous Materials with Independent Control of the Dual Pore Size Distribution. *Chem. Commun.* **2001**, *24*, 2670–2671. https://doi.org/10.1039/b108860b.

(37) Sun, J. H.; Shan, Z.; Maschmeyer, T.; Coppens, M. O. Synthesis of Bimodal Nanostructured Silicas with Independently Controlled Small and Large Mesopore Sizes. *Langmuir* **2003**, *19* (20), 8395–8402. https://doi.org/10.1021/la0351156.

(38) Zhao, S.; Zhang, Y.; Zhou, Y.; Sheng, X.; Zhang, C.; Zhang, M.; Fang, J. One-Step Synthesis of Core-Shell Structured Mesoporous Silica Spheres Templated by Protic Ionic Liquid and CTAB. *Mater. Lett.* **2016**, *178*, 35–38. https://doi.org/10.1016/j.matlet.2016.04.182.

(39) Gao, H.; Zhou, Y.; Sheng, X.; Zhao, S.; Zhang, C.; Zhang, M. Synthesis of Core-Shell and Hollow Structured Dual-Mesoporous Silica Templated by Alkoxysilyl-Functionalized Ionic Liquids and CTAB. *Mater. Lett.* **2018**, *211*, 126–129. https://doi.org/10.1016/j.matlet.2017.09.067.

(40) Wang, X.; Zhou, L.; Liu, Y.; Yin, S.; Qiao, Z. A.; Huo, Q. Transformation from Single-Mesoporous to Dual-Mesoporous Organosilica Nanoparticles. *Nanoscale* **2017**, *9* (19), 6362–6369. https://doi.org/10.1039/c7nr00363c.

(41) Lee, J. H.; Kang, S.; Ahn, M.; Jang, H.; Min, D. H. Development of Dual-Pore Coexisting Branched Silica Nanoparticles for Efficient Gene–Chemo Cancer Therapy. *Small* **2018**, *14* (7), 1–7. https://doi.org/10.1002/smll.201702564.

(42) Park, D. K.; Ahn, J. H. Synthesis of Double Mesoporous Silica Nanoparticles and Control of Their Pore Size 이중 다공성 실리카 나노입자 합성 및 공극 크기 조절. **2021**, *1* (1), 167–169. https://doi.org/10.18770/KEPCO.2021.07.01.167.

(43) Qin, L.; Niu, D.; Li, N.; Luo, X.; Qin, X.; Chen, J.; Li, Y.; Shi, J. Hydrophobicity-Induced Electrostatic Interfacial Self-Assembly for Porous Silica Nanospheres with Tunable Pore Sizes and Pore Hierarchies. *Chem. Eng. J.* **2021**, *405*, 126936. https://doi.org/https://doi.org/10.1016/j.cej.2020.126936.

(44) Brown, P.; Butts, C. P.; Eastoe, J. Stimuli-Responsive Surfactants. *Soft Matter* **2013**, *9* (8), 2365–2374. https://doi.org/10.1039/c3sm27716j.

(45) Holmberg, K. Surfactants with Controlled Half-Lives. *Curr. Opin. Colloid Interface Sci.* **1996**, *1* (5), 572–579. https://doi.org/10.1016/s1359-0294(96)80094-x.

(46) Cabane, E.; Zhang, X.; Langowska, K.; Palivan, C. G.; Meier, W. Stimuli-Responsive Polymers and Their Applications in Nanomedicine. *Biointerphases* **2012**, *7* (1–4), 1–27. https://doi.org/10.1007/s13758-011-0009-3.

(47) Shukla, D.; Tyagi, V. K. Development of Cleavable Surfactants. *Tenside, Surfactants, Deterg.* **2010**, *47* (1), 7–12. https://doi.org/10.3139/113.110046.

(48) Ghosh, S.; Irvin, K.; Thayumanavan, S. Tunable Disassembly of Micelles Using a Redox Trigger. *Langmuir* **2007**, *23* (15), 7916–7919. https://doi.org/10.1021/la700981z.

(49) Bej, R.; Dey, P.; Ghosh, S. Disulfide Chemistry in Responsive Aggregation of Amphiphilic

Systems. *Soft Matter* **2019**, *16* (1), 11–26. https://doi.org/10.1039/c9sm01960j.

(50) Stjerndahl, M.; Lundberg, D.; Chauhan, V.; Bordes, R.; Holmberg, K. Cleavable Surfactants: A Comparison between Ester, Amide, and Carbonate as the Weak Bond. *J. Surfactants Deterg.* **2019**, *22* (5), 1139–1145. https://doi.org/10.1002/jsde.12247.

(51) Lundberg, D.; Stjerndahl, M.; Holmberg, K. Surfactants Containing Hydrolyzable Bonds. In *Interfacial Processes and Molecular Aggregation of Surfactants*; Springer, 2008; pp 57–82.

(52) Bochet, C. G. Photolabile Protecting Groups and Linkers. *J. Chem. Soc. Perkin Trans. 1* **2002**, No. 2, 125–142. https://doi.org/DOI https://doi.org/10.1039/B009522M.

(53) Sebastian Blackwood. Thermolabile Protecting Groups in Metal-Organic Frameworks, PhD Thesis, Massey University, Manawatu, New Zealand, 2016.

(54) Huang, Y.; Thanneeru, S.; Zhang, Q.; He, J. A New Design of Cleavable Acetal-Containing Amphiphilic Block Copolymers Triggered by Light. *J. Polym. Sci. Part A Polym. Chem.* **2018**, *56* (16), 1815–1824. https://doi.org/10.1002/pola.29062.

(55) Picchetti, P.; Dimarco, B. N.; Travaglini, L.; Zhang, Y.; Ortega-Liebana, M. C.; De Cola, L. Breaking with Light: Stimuli-Responsive Mesoporous Organosilica Particles. *Chem. Mater.* **2020**, *32* (1), 392–399. https://doi.org/10.1021/acs.chemmater.9b03937.

(56) Attwood, D. *Surfactant Systems: Their Chemistry, Pharmacy and Biology*; Springer Science & Business Media, 2012.

(57) Barnes, G., Gentle, I. *Interfacial Science: An Introduction*; Oxford university press, 2011.

(58) Biolin Scientific. Biolin Scientific https://www.biolinscientific.com/.(accessed on 14/11/2022)

(59) M. J. Frisch, G. W. Trucks, H. B. Schlegel, G. E. Scuseria, M. A. Robb, J. R. Cheeseman, G. Scalmani, V. Barone, B. Mennucci, G. A. Petersson, H. Nakatsuji, M. Caricato, X. Li, H. P. Hratchian, A. F. Izmaylov, J. Bloino, G. Zheng, J. L. Sonnenberg, M. Had, and D. J. F. Gaussian 09. Gaussian, Inc.: Wallingford CT 2009.

(60) Ho, H. T.; Phan, T. N. T.; Bonnevide, M.; Malicki, N.; Couty, M.; Jestin, J.; Gigmes, D. Photolabile Well-Defined Polystyrene Grafted on Silica Nanoparticle via Nitroxide-Mediated Polymerization (NMP). *Macromol. Rapid Commun.* **2021**, *42* (18), 1–5. https://doi.org/10.1002/marc.202100181.

(61) Schumers, J.-M.; Gohy, J.-F.; Fustin, C.-A. A Versatile Strategy for the Synthesis of Block Copolymers Bearing a Photocleavable Junction. *Polym. Chem.* **2010**, *1* (2), 161–163. https://doi.org/10.1039/B9PY00218A.

(62) Gaplovsky, M.; Il'ichev, Y. V; Kamdzhilov, Y.; Kombarova, S. V; Mac, M.; Schwörer, M. A.; Wirz, J. Photochemical Reaction Mechanisms of 2-Nitrobenzyl Compounds: 2-Nitrobenzyl Alcohols Form 2-Nitroso Hydrates by Dual Proton Transfer. *Photochem. Photobiol. Sci.* **2005**, *4* (1), 33–42. https://doi.org/https://doi.org/10.1039/B409927C.

(63) Wang, M.; Jiang, X. Sulfur–Sulfur Bond Construction. *Top. Curr. Chem.* **2018**, *376* (2), 14. https://doi.org/10.1007/s41061-018-0192-5.

(64) Qiu, X.; Yang, X.; Zhang, Y.; Song, S.; Jiao, N. Efficient and Practical Synthesis of Unsymmetrical Disulfides: Via Base-Catalyzed Aerobic Oxidative Dehydrogenative Coupling of Thiols. *Org. Chem. Front.* **2019**, *6* (13), 2220–2225. https://doi.org/10.1039/c9qo00239a.

(65) Ren, S.; Luo, N.; Liu, K.; Liu, J.-B. Synthesis of Unsymmetrical Disulfides via the Cross-Dehydrogenation of Thiols. *J. Chem. Res.* **2021**, *45* (5–6), 365–373. https://doi.org/https://doi.org/10.1177/1747519820942872.

(66) Huang, P.; Wang, P.; Tang, S.; Fu, Z.; Lei, A. Electro-oxidative S− H/S− H Cross-coupling with Hydrogen Evolution: Facile Access to Unsymmetrical Disulfides. *Angew. Chemie* **2018**, *130* (27), 8247–8251. https://doi.org/https://doi.org/10.1002/ange.201803464.

(67) Shao, H.; Jiang, L.; Meng, W.-D.; Qing, F.-L. Synthesis and Antimicrobial Activity of a

Perfluoroalkyl-Containing Quaternary Ammonium Salt. *J. Fluor. Chem.* **2003**, *124* (1), 89–91. https://doi.org/10.1016/S0022-1139(03)00193-3.

(68)   Cheng, Y.-J.; Zhang, A.-Q.; Hu, J.-J.; He, F.; Zeng, X.; Zhang, X.-Z. Multifunctional Peptide-Amphiphile End-Capped Mesoporous Silica Nanoparticles for Tumor Targeting Drug Delivery. *ACS Appl. Mater. Interfaces* **2017**, *9* (3), 2093–2103. https://doi.org/https://doi.org/10.1021/acsami.6b12647.

(69)   Zhai, H.; Wang, Y.; Wang, M.; Liu, S.; Yu, F.; Gao, C.; Li, G.; Wu, Q. Construction of a Glutathione-Responsive and Silica-Based Nanocomposite for Controlled Release of Chelator Dimercaptosuccinic Acid. *Int. J. Mol. Sci.* **2018**, *19* (12), 3790. https://doi.org/https://doi.org/10.3390/ijms19123790.

(70)   Cleland, W. W. Dithiothreitol, a New Protective Reagent for SH Groups. *Biochemistry* **1964**, *3* (4), 480–482. https://doi.org/https://doi.org/10.1021/bi00892a002.

(71)   Maggini, L.; Cabrera, I.; Ruiz-Carretero, A.; Prasetyanto, E. A.; Robinet, E.; De Cola, L. Breakable Mesoporous Silica Nanoparticles for Targeted Drug Delivery. *Nanoscale* **2016**, *8* (13), 7240–7247. https://doi.org/10.1039/C5NR09112H.

(72)   Jiang, X.; Mu, H.; Hsieh, Y.-H. P.; Rao, Q. Isolation and Characterization of Chicken Serum Albumin (Hen Egg Alpha-Livetin, Gal d 5). *Foods* **2022**, *11* (11), 1637. https://doi.org/https://doi.org/10.3390/foods11111637.

(73)   Mthembu, S. N.; Sharma, A.; Albericio, F.; de la Torre, B. G. Breaking a Couple: Disulfide Reducing Agents. *ChemBioChem* **2020**, *21* (14), 1947–1954. https://doi.org/https://doi.org/10.1002/cbic.202000092.

(74)   Handbook, G.-B. D. *Selection Guide to Detergents & Detergent Removal*; G-Biosciences: April, 2015.

(75)   Hammouda, B. Analysis of the Beaucage Model. *J. Appl. Crystallogr.* **2010**, *43* (6), 1474–1478. https://doi.org/https://doi.org/10.1107/S0021889810033856.

(76)   Chu, B. *Laser Light Scattering: Basic Principles and Practice*; Courier Corporation, 2007.
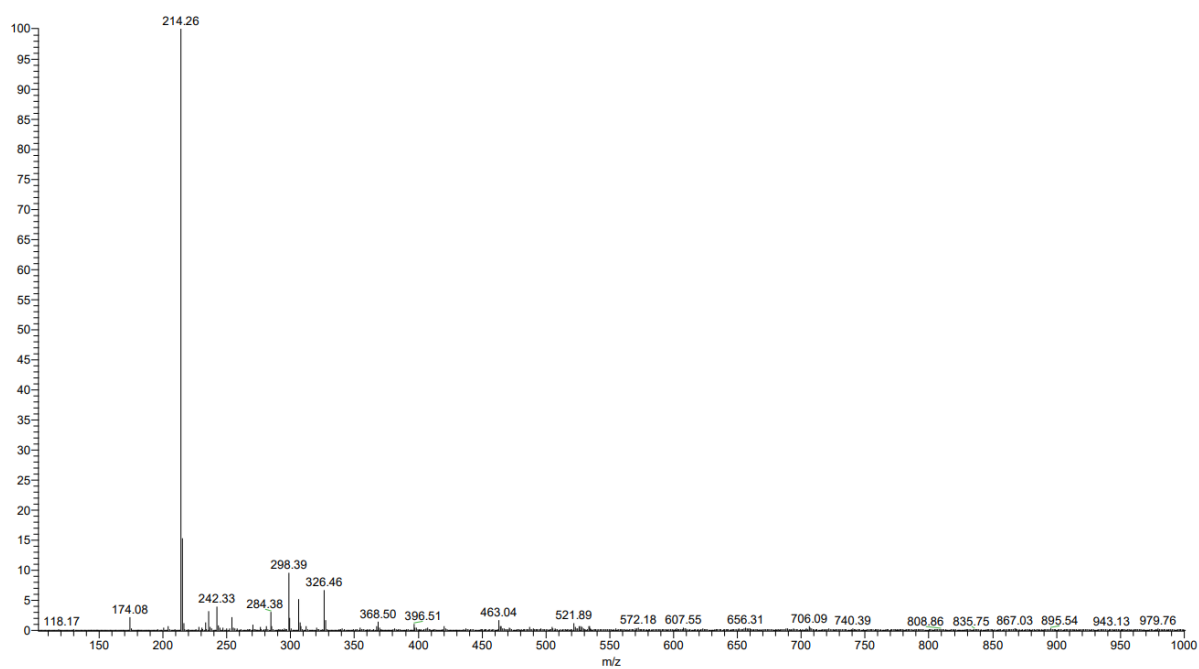
Appendix A- Mass and NMR spectra
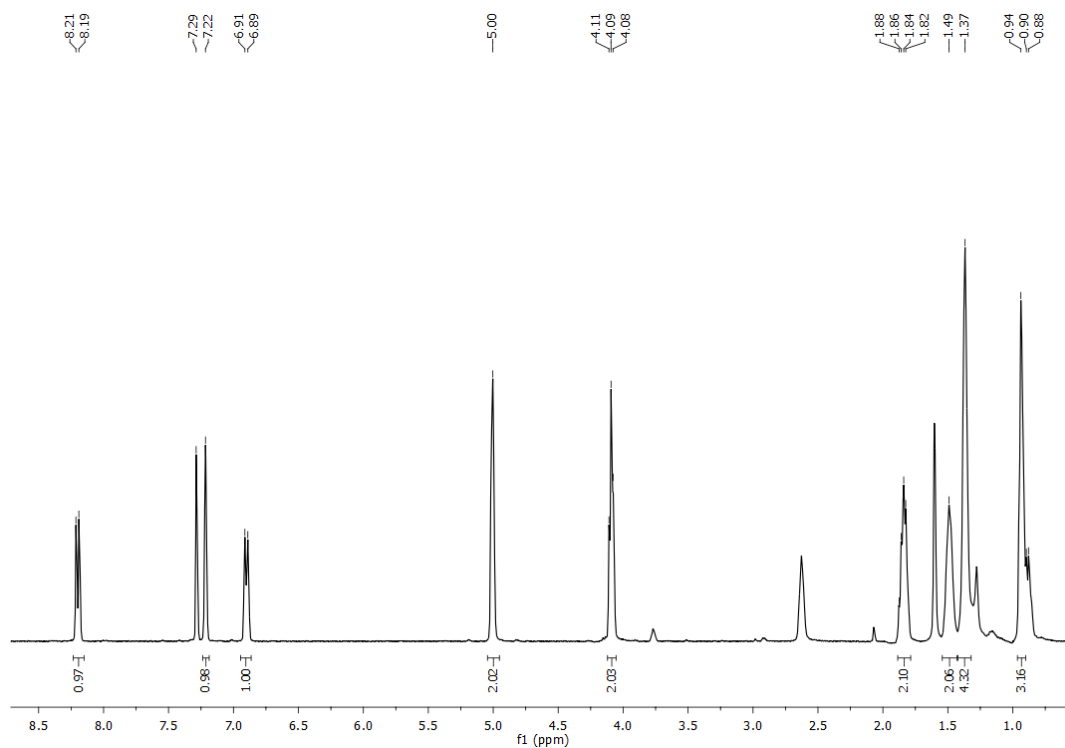

Figure A.1. *ESI⁺-MS spectrum of compound **1**.*

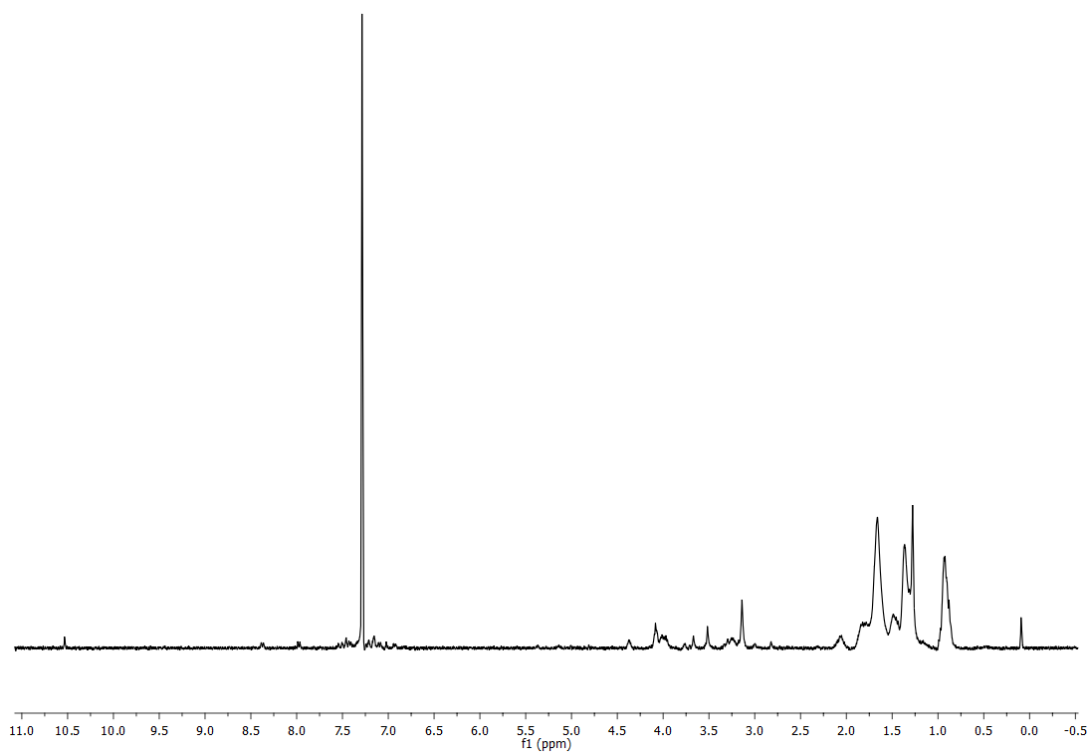**Figure A.2.** *¹H NMR spectrum of Fraction 2 from Attempt 1 to achieve the light- responsive surfactant (compound **2**), in CDCl₃.*

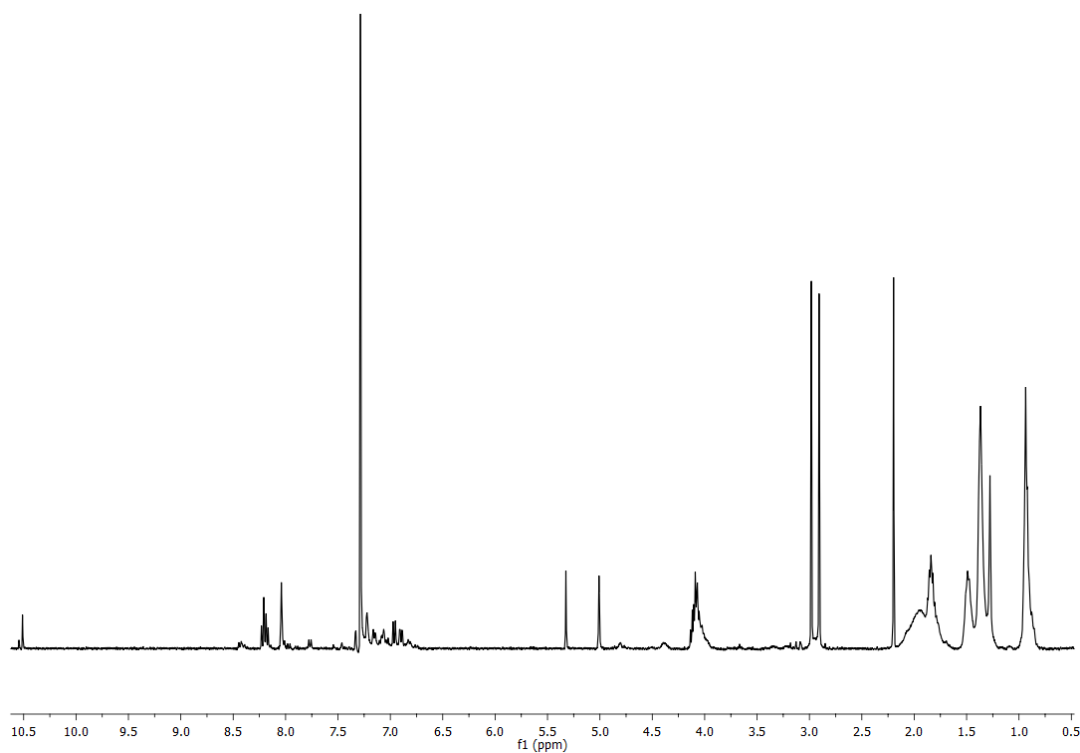**Figure A.3.** ^{1}H NMR spectrum of Fraction 3 from Attempt 1 to achieve the light- responsive surfactant (compound **2**), in CDCl_3.

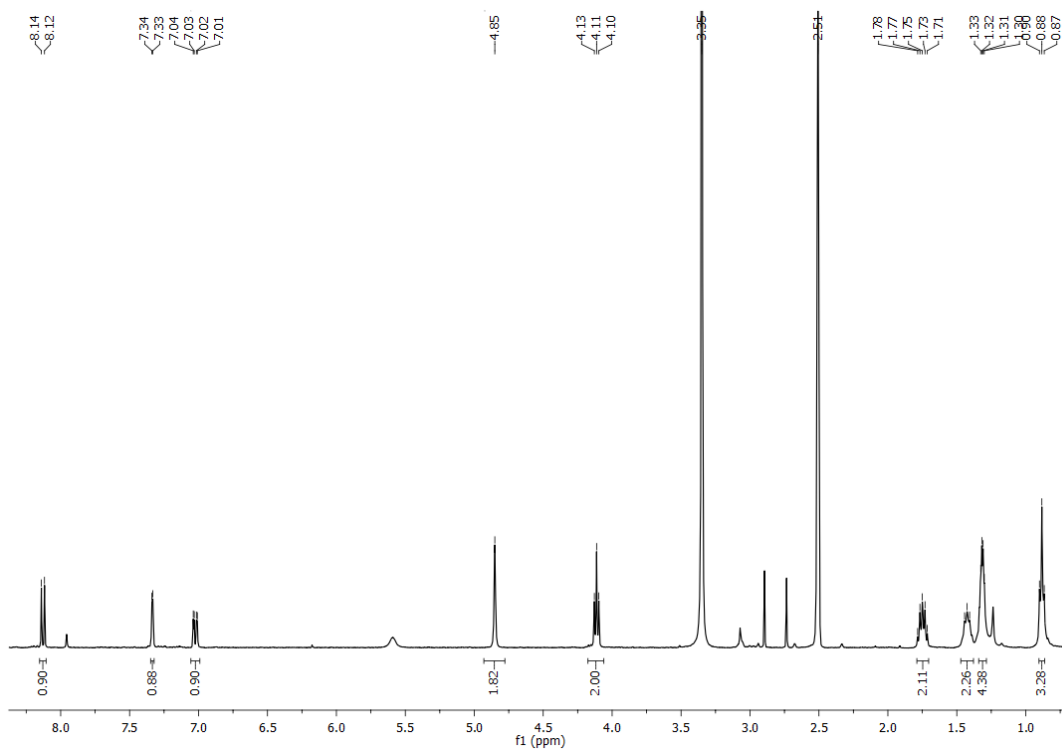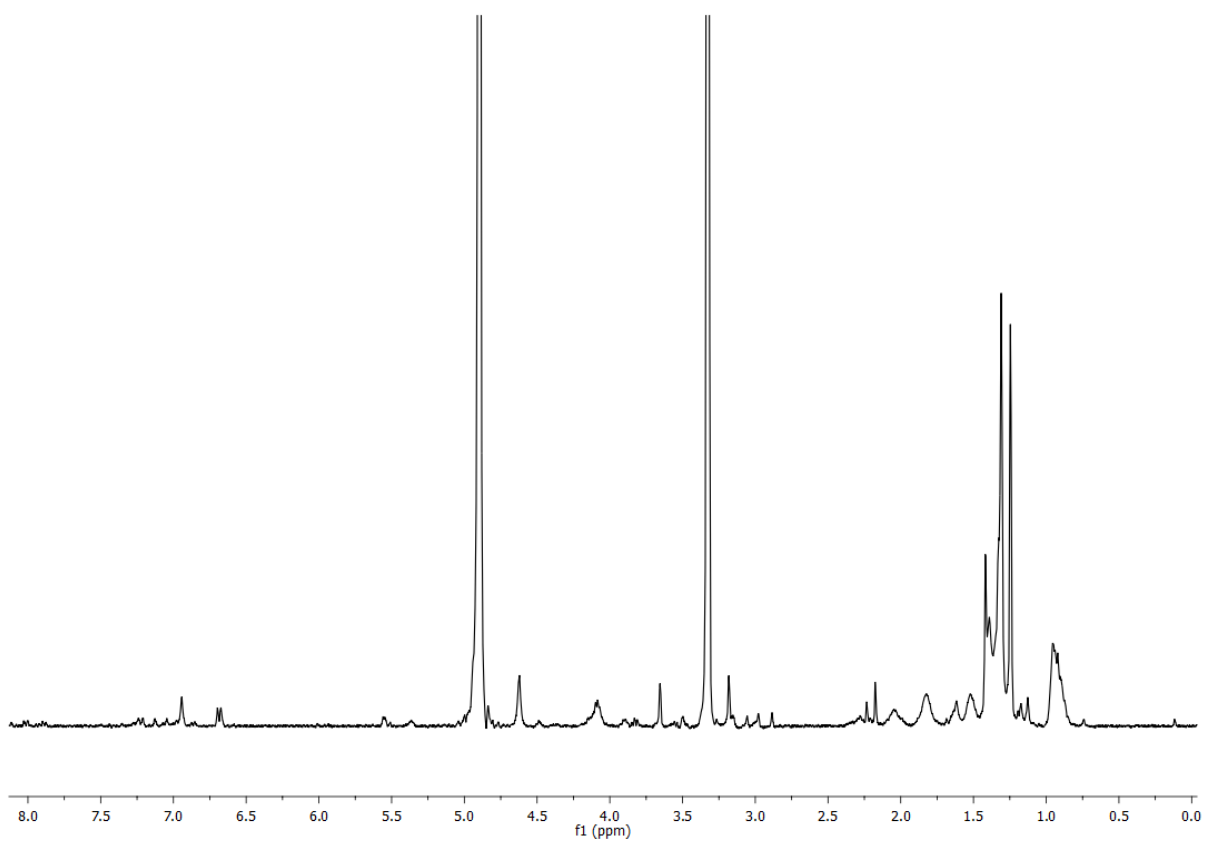**Figure A.4.** ^{1}H NMR spectrum of Attempt 2 to achieve the light- responsive surfactant (compound **2**), in CDCl_3.

Figure A.5. ^1H NMR spectrum of Attempt 3 to achieve the light- responsive surfactant (compound **2**), in DMSO-d_6.
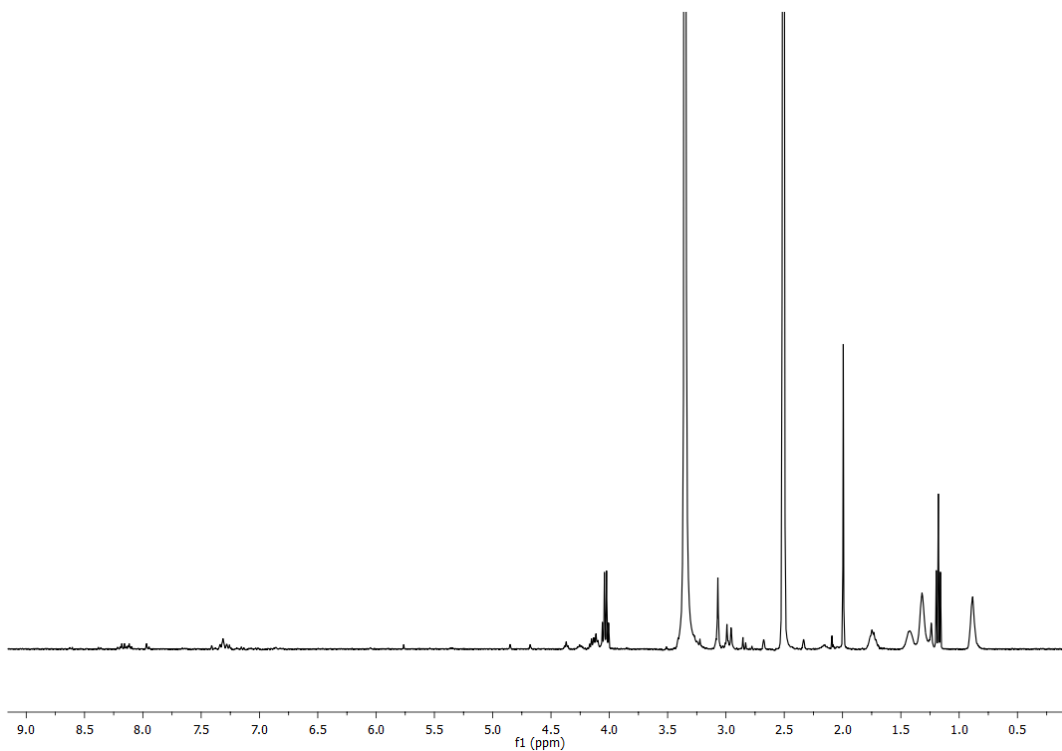
Figure A.6. ^1H NMR spectrum of Attempt 4 to achieve the light- responsive surfactant (compound **2**), in DMSO-d_6.

61
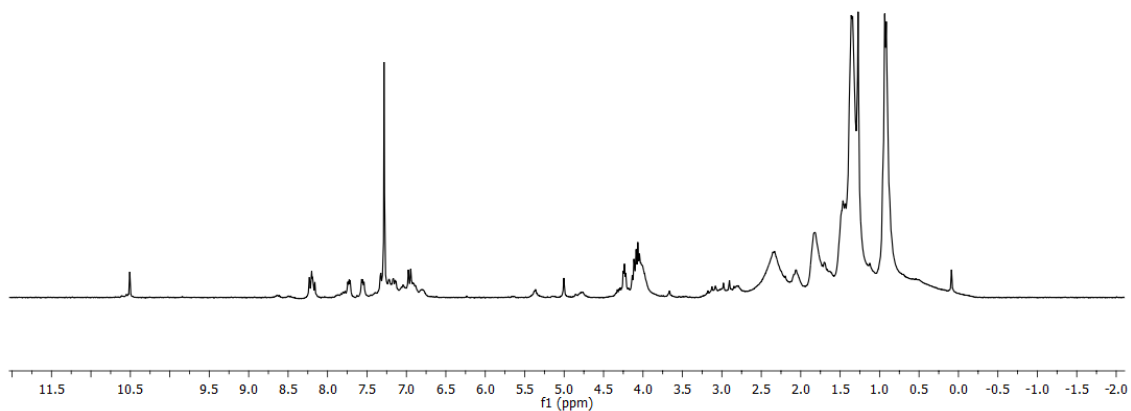
Figure A.7. ^{1}H NMR spectrum of Attempt 5 to achieve the light- responsive surfactant (compound **2**), in CDCl$_3$.

Figure A.8. ^{1}H NMR spectrum of Attempt 6 to achieve the light- responsive surfactant (compound **2**), in MeOD.
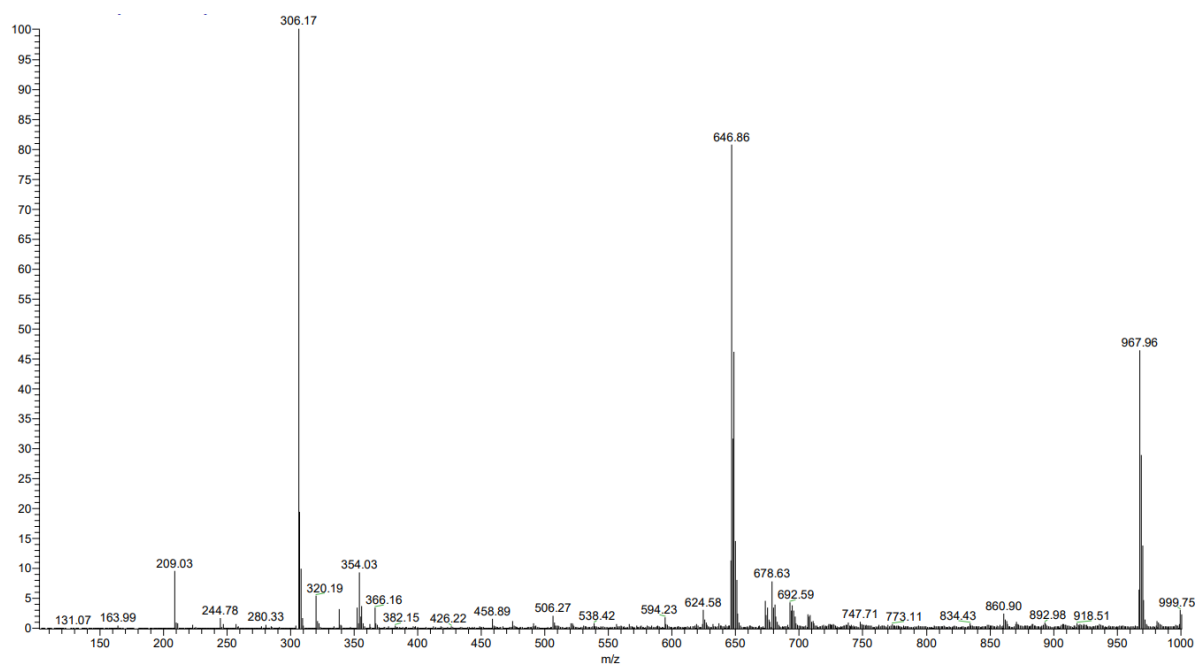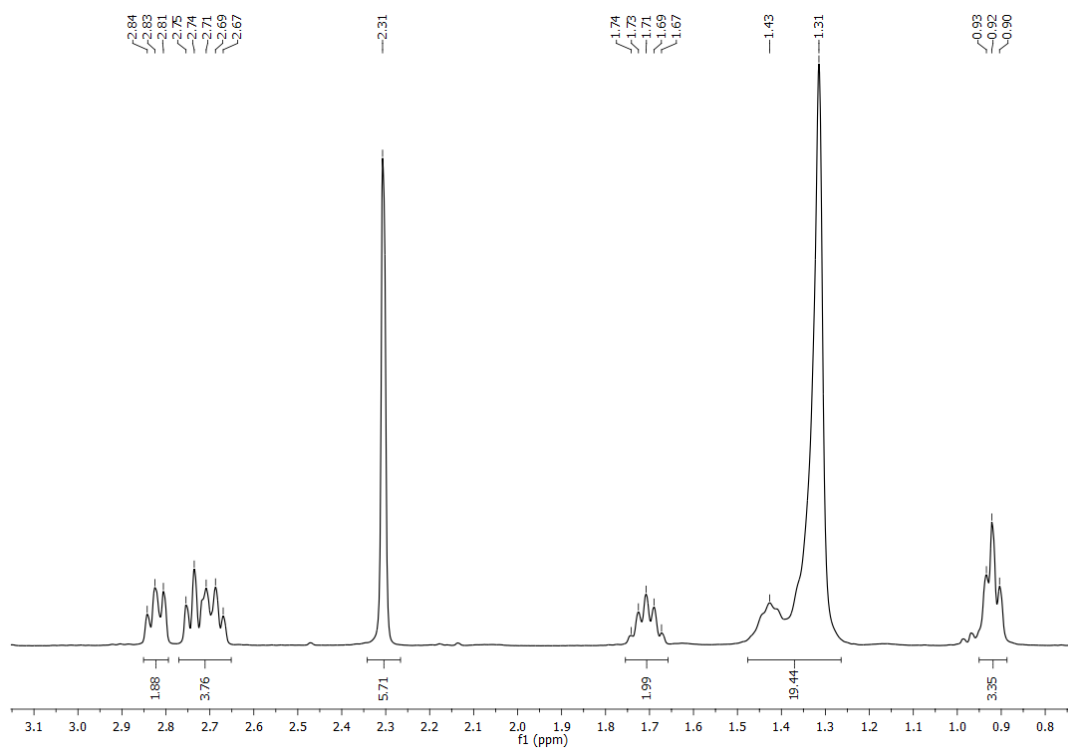
Figure A.9. *ESI⁺-MS spectrum of compound* **3**.

Figure A.10. *¹H NMR spectrum of compound* **3** *in MeOD.*
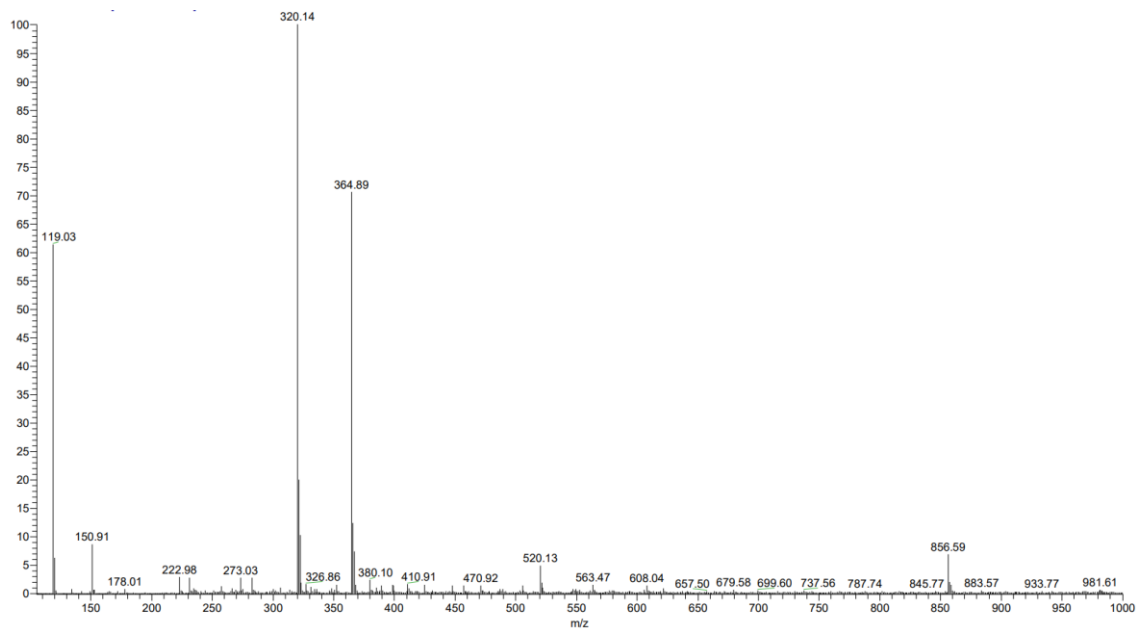
Figure A.11. *ESI⁺-MS spectrum of compound 4.*
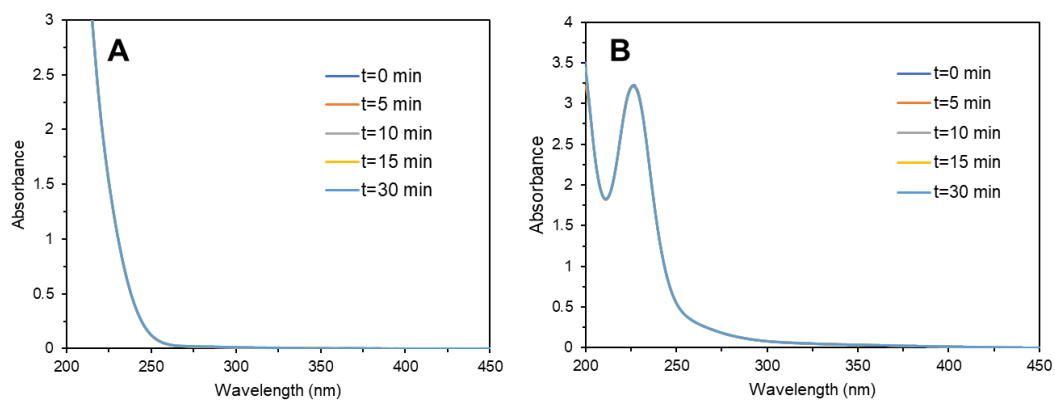
Appendix B- Preliminary studies with CTAC-SS

Figure B.1. *Absorption spectra of aqueous solutions of DTT (5mM) (**A**) and CTAC-SS (1.25 mM) (**B**) at pH 7.*